

UNIVERSITY OF OKLAHOMA

GRADUATE COLLEGE

MICROSTRUCTURAL STUDY OF MUCIN: INFLUENCE OF PH,  
TEMPERATURE, CONCENTRATION AND NANOPARTICLES

A THESIS

SUBMITTED TO THE GRADUATE FACULTY

in partial fulfillment of the requirements for the

Degree of

MASTER OF SCIENCE

By

ONYINYECHI IGWE

Norman, Oklahoma

2020

MICROSTRUCTURAL STUDY OF MUCIN: INFLUENCE OF PH,  
TEMPERATURE, CONCENTRATION AND NANOPARTICLES

A THESIS APPROVED FOR THE  
SCHOOL OF CHEMICAL, BIOLOGICAL AND MATERIALS ENGINEERING

BY THE COMMITTEE CONSISTING OF

Dr. Keisha B. Walters, Chair

Dr. Sepideh Razavi

Dr. Jie Gao

© Copyright by ONYINYECHI IGWE 2020

All Rights Reserved.

## Table of Contents

Table of Contents .....	iv
Acknowledgements .....	vi
Abstract .....	viii
Chapter 1. Introduction .....	1
1.3 Importance of Mucin Studies .....	2
1.4 Study Goals and Organization.....	2
Chapter 2. Monitoring The Influence of Concentration, Temperature, and pH Changes in Mucin Microstructure.....	3
2.1. Abstract .....	3
2.2. Introduction .....	3
2.3. Materials and Methods .....	4
2.4. Results and Discussion.....	6
2.5. PGM Temperature and Concentration Studies.....	7
2.6. PGM pH Studies.....	15
2.7. Conclusions .....	21
Chapter 3. Effect of Silica Nanoparticle Addition on Mucin Microstructure.....	23
3.1. Abstract .....	23
3.2. Introduction .....	23
3.3. Materials and Methods.....	25
3.4. Results and Discussion.....	29
3.5. Conclusions .....	36
Chapter 4. Effect of Magnetic Nanoparticle Addition on Mucin Microstructure.....	37
4.1. Abstract .....	37
4.2. Introduction .....	37
4.3. Materials and Methods.....	38
4.4. Results and Discussion.....	42
4.5. Conclusions .....	49
Chapter 5. Conclusions and Future Work.....	50
5.1. Study Conclusions.....	50
5.2. Future Work Recommendations.....	51
Appendices.....	52

Appendix A: Sample Preparation Methods.....	52
A1. Mucin Solutions.....	52
A2. Mucin pH solutions .....	52
Appendix B: Operating Procedures.....	53
B1. Surface Tension .....	53
B2. Rheology .....	54
B3. Dynamic Light Scattering.....	55
B4. Zeta Potential .....	57
B5. Fourier Transform Infrared Spectroscopy (FTIR) .....	58
Works Cited .....	67

## Acknowledgements

I would like to thank my advisor Dr. Keisha Walters for your mentorship, support, patience, and encouragement throughout my program. Thank you for believing in me and working very hard to ensure that I made it to the end.

Thank you to the members of the Polymer and Surface Engineering Laboratories (PolySEL) research group. In particular, I appreciate Kayla Foley sparking my interest in research during my sophomore year of college and mentoring me as an undergraduate researcher. Thank you for always making time to answer my questions, brainstorm ideas with me, and teach me new things both in the lab and classroom. Brandon Abbott, thank you for supporting these efforts through silica and magnetic nanoparticle synthesis, characterization, and preparation. Thank you also for being a great friend, motivator, and study partner. Finally, many thanks to Collin Britten- for being so kind and willing to lend a helping hand at all times.

Thank you OU alum and University of Michigan Ph.D. candidate Kaylee Smith for your major contribution to the silicon nanoparticle work. As an undergraduate researcher at OU, Kaylee worked with Austin Curnutt to conduct experiments on mucin rheology and provided characterization of the silica nanoparticle doped mucin solutions. Thank you also for always responding to my many emails, texts and calls.

Thank you Brittney Miles, an undergraduate researcher for helping me with sample preparation and dynamic light scattering experiments. Thank you to Lucas Condes, another undergraduate researcher for assisting me with zeta potential experiments.

Thank you Rae Lane, for her contribution to my papers through her art work.

Thank you to CBME Research Scientist, Andrew D'Amico, for always lending a helping hand to help fix and troubleshoot equipment, lending me his personal tools to further my research, and brainstorming ideas with me. I really appreciate you.

Thank you to my committee members, Dr. Sepideh Razavi and Dr. Jie Gao, for agreeing to serve as my committee members and being flexible with your schedules.

Thank you to my family for your endless love, support and understanding during stressful times. Thank you also for always checking in to make sure I was okay.

Thank you to my well-wishers and friends, Idinma Illodibe, Jonathan Ifegunni, Minji Zdeb, Alondra Martinez, Beatrice Alcala, and Courtney Duckett, for always being there for me in good and bad times. Thank you for always listening, being understanding, and supporting me throughout this journey. I love you all dearly.

## Abstract

The aim of this research is to examine the nano- and micro-structure of mucin in response to chemico-physical changes within the aqueous solution. By characterizing the mucin structure across a range of length scales relationships can be developed and related to the macroscopic properties. Mucin is a glycoprotein found in mucus at very low concentrations but yet is responsible for the majority of the physical properties of mucus. Therefore, the biological behavior (e.g., barrier properties) of mucus can be related to the reversible structural changes—viable dynamic bonding—that occurs within and between mucin strands. In the present work, the impact of pH, temperature and nanoparticle addition were examined on the structure of porcine gastric mucin (PGM) in aqueous solution. Findings are presented regarding the influence of (i) temperature and concentration on mucin aggregation and gelling properties, (ii) pH on surface tension, aggregation, and network structure, and (iii) addition of silica nanoparticles (SiNPs) and magnetic nanoparticles (MNPs) on mucin aggregation and rheology.

The samples were characterized using rheology, dynamic light scattering (DLS) particle measurements, zeta potential (ZP), Fourier-transform infrared spectroscopy (FTIR), and pendant drop surface tension measurements. Rehydrated purified mucin is used in this study as it is structurally comparable to native mucus and readily available. Mucin concentrations were examined at 1, 2, and 5 wt% for the pH and temperature study. For the nanoparticle experiments, the mucin concentration was held constant at 1 wt% and the nanoparticle concentration varied. It is shown that changes in the microstructure of PGM due to concentration, temperature, and pH can be observed through surface tension, rheological, DLS, and ZP measurements. By varying the pH, the PGM solution could be induced to undergo a sol-gel transition, and PGM strands were found to aggregate and form a network structure under acidic conditions. DLS and ZP data showed that at the isoelectric point, PGM displayed the largest mean diameter by number as is expected when there is no longer charge repulsion and aggregation is induced. Increased temperature and concentration also influenced the viscoelastic properties of the mucin solutions. The sol-gel transition was observed to occur at higher frequencies for samples at higher PGM concentrations and temperatures. Finally, nanoparticle interaction with PGM showed an increase in gelling behavior and swelling of mucin in solution.



# Chapter 1. Introduction

## *1.1 Abstract*

This thesis is constructed of related but distinct studies regarding the chemical-microstructure of mucin solutions as the chemical composition is changed. The work presented will examine the impact of pH, temperature and the addition of silica and iron oxide nanoparticles. Accordingly, the thesis is organized by chapters according to these respective foci. This first chapter serves as a short summary of the subject and to layout the organization of the remainder of the thesis.

## *1.2 Definition and Function of Mucin*

Mucus is a hydrogel that coats and protects all wet epithelia including the eyes and the respiratory, gastrointestinal, and cervicovaginal tracts. It forms a selectively permeable layer that permits the passage of some materials while restricting others, and it also serves as lubricating and protectant of the underlying epithelial surface.<sup>1</sup> Because of its location and properties, mucus is an arena for microbe collection in the body and it is also a primary option for targeted drug delivery especially those directed at the treatment of underlying tissues and organs.

Mucus is comprised of 75% carbohydrates and 25% amino acids and linked together by O-glycosidic bonds between N-acetylgalactosamine and serine or threonine residues.<sup>2</sup> However, there is limited availability of mucus for research that has been collected from humans and other mammals. In addition, significant patient-to-patient variability has been observed which prevents a systematic study of the effect of chemical composition.<sup>3</sup> Solutions made from purified mucins, such as porcine gastric mucus (PGM), exhibit important features of native mucus, including characteristic viscoelastic and selective barrier properties<sup>4,5</sup> and specific interactions with mucosal microbes.<sup>6,7</sup> Hence, purified mucins may serve as a simplified model environment for the study of mucus.

### *1.3 Importance of Mucin Studies*

Studying the surface tension of mucin is very important because this will help us understand how mucin in the body behaves under certain conditions. This research is very useful in pharmaceutical and drug delivery applications to understand the interaction between the mucin of a patient with a mucus related condition and the drug being administered. The alteration of PGM using small molecules and nanoparticles in vitro is an area of interest in drug delivery research. Understanding the structure and behavior of mucin can lead to the discovery of better drug delivery methods or a potential cure for mucus related conditions like cystic fibrosis (CF), ulcerative colitis, and chronic obstructive pulmonary disease (COPD).

### *1.4 Study Goals and Organization*

The overall goal of this research is to study how chemico-physical changes affect the nano- and micro-structure of mucin and the relationship between those small length scale structures and the macroscopic properties. Specifically, mucin—as a biopolymer—is an amphiphilic macromolecule capable of reversible ionic bonding within a single chain (intrachain conformation changes) or between adjacent chains. Through interchain interactions, mucin is capable of forming network structures that connect from the nanoscale to the microscale and ultimately the macroscale properties of mucin solutions and mucus. The ability to relate the microstructure (and nanostructure) to the more readily available measurement methods for macroscale properties (e.g. viscosity) will provide insight into the behaviors of mucin solutions and other complex fluids.

This effort builds upon prior efforts in our group on mucus<sup>8-10</sup>, mucin solutions<sup>8, 11</sup>, and rheology of charged polymers<sup>12-14</sup>. The present work extends our prior knowledge by examining the effect of pH and difference in properties at ambient and physiological temperature (Chapter 2). The addition of nanoparticles to mucus (and mucin solutions) has been examined in response to particle inhalation related to pollution, industrial exposure, and drug delivery. Chapters 3 and 4 examine the effects of adding nanoparticles to the mucin solution to examine if the nanoparticles disrupt mucin-mucin interactions and resulting in a breakdown of the network structure. Chapter 5 discusses the overall conclusions from this project, along with future directions. Ancillary information is provided in the appendices, including descriptions of the experimental procedures.

## **Chapter 2. Monitoring The Influence of Concentration, Temperature, and pH Changes in Mucin Microstructure**

### *2.1. Abstract*

In this study surface tension, rheology, dynamic light scattering (DLS), and zeta potential (ZP) methods have been utilized to examine the microstructural changes in porcine gastric mucin (PGM) when concentration, temperature and pH are varied. DLS and ZP measurements on dilute solutions of mucin disclosed maximum aggregation due to absence of inter-particle repulsive forces at the isoelectric point (pH 3). Surface tension values increase as mucin becomes more acidic and the network structure is more constricted. Temperature rheology studies at 25 °C and 37 °C show that PGM samples require higher frequencies at elevated temperatures to overcome the sol-gel transition. The findings show that changes in the microstructure of PGM due to concentration, temperature, and pH changes can be studied and observed through surface tension, rheological, and size and charge distribution experiments.

### *2.2. Introduction*

Mucus is a hydrogel that coats and protects all wet epithelia, including the eyes and the respiratory, gastrointestinal, and cervicovaginal tracts. It is a selectively permeable layer that permits the passage of some substrates while restricting others, protecting the underlying epithelial surface.<sup>1</sup> Because of this, mucus is the primary arena for microbes in the body and is a suitable medium to use for targeted drug delivery of mucus related conditions. The surface tension, rheological properties and particle properties are crucial to its protective function and important for drug delivery applications through the mucin layer. Varying the pH of PGM using buffers in vitro is a special area of interest in drug delivery research to better understand how gastric mucin behaves in regular (acidic) conditions and under abnormal circumstances.

This study aims to explore microstructural changes in the properties of gastric mucin for drug delivery applications. This was done by varying concentration, pH, and temperatures of PGM samples and using several analytical techniques to study its behavior under different conditions. Studying the properties of gastric mucins such as PGM is very important because this help us further understand how mucin in the body behaves under certain conditions. Purified mucins such

as porcine gastric mucus (PGM) exhibit important features of native mucus, including characteristic viscoelastic and selective barrier properties<sup>4,5</sup> and specific interactions with mucosal microbes.<sup>6,7</sup> Hence, purified mucins may serve as a simplified model environment for the study of mucin. In this article, surface tension using the pendant drop method and bubble pressure is evaluated to be an appropriate method to recognize microstructural changes in PGM. Using information derived from surface tension measurements, dynamic light scattering (DLS), rheology and zeta potential (ZP) are also carried out to evaluate and study the physical and interaction properties at areas where the surface tension data suggests changes in PGM microstructure. These experiments provided particle sizing, sol-gel transition and zeta potential data that are critical to understanding the interaction of gastric mucin with drugs or bacteria. Understanding the structure and behavior of mucin under different conditions can lead to the discovery of more effective drug delivery methods or a potential cure for mucus related conditions like cystic fibrosis (CF), ulcerative colitis, and chronic obstructive pulmonary disease (COPD).

### *2.3. Materials and Methods*

*PGM Solutions.* Solutions of PGM (porcine gastric mucin, Type II, Sigma Aldrich, CAS No. 84082-64-4) were prepared at 1, 2, and 5 mg/mL concentrations using filtered Nanopure™ water. PGM solutions were sonicated for 1 hour and then refrigerated for 24 hours prior to characterization to ensure the mucin was thoroughly hydrated. The refrigerated samples were allowed to warm to room temperature on a bench-top and sonicated for 30 minutes just before experiments were carried out to ensure the samples were well mixed.

For surface tension measurements, several common solvents were used as controls to allow for comparison of measured surface tensions with literature values. In this study, these controls included Nanopure™ water, pyridine, and hexadecane. The water was produced in house using a Millipore Synergy® Water Purification System #SYNS0HFUS with an EMD Millipore CDUFBI001 Biopak Ultrafiltration Cartridge, and the pyridine and hexadecane were purchased from Sigma Aldrich (95+%, used as received). These three solvents were chosen because they span a wide range of surface tensions and charges. Nanopure™ water is highly polar, hexadecane is highly nonpolar, and pyridine model compound with both polar and dispersive components.

Pendant Drop. Surface tension measurements at room temperature were collected using a Krüss Drop Shape Analyzer-DSA25. This was used to measure the surface tension of PGM at three different concentrations (1, 2, and 5 mg/mL), and three different solvents to determine accuracy of the method, and to ensure that it can handle all types of solutions. Before experiments, the instrument was calibrated by adjusting the camera focus, specifying the needle diameter, selecting the region of interest, and setting the measuring lines. A 0.51mm diameter needle was used for pendant drop experiments. After drops were dispensed, a wait time of 30 seconds was observed before collecting data. All error for data is shown as 95% confidence intervals.

pH Study. pH studies were conducted on PGM samples. The acid used was 0.01 M nitric acid (HNO<sub>3</sub>) and the base was 0.01 M sodium hydroxide (NaOH). Drops of these samples were added to the PGM solutions to change their pH and the surface tensions were measured using a Krüss Drop Shape Analyzer-DSA25. The pH meter used when preparing the samples is a Thermo Scientific™ Orion™ Dual Star™ pH and ISE Benchtop Meter.

Rheology. Rheological measurements were collected using a TA instruments Discovery Hybrid Rheometer II using Trios software (v5.00). A 40 mm cone with an angle of 2.013° was used to perform frequency and flow sweeps on the solutions containing PGM at various concentrations. The angled 40 mm geometry was chosen because the diameter was appropriate for samples with medium viscosity and the cone shape produces a smaller gap height closer to inside so the shear on the sample is constant.<sup>15</sup>

Before rheological measurements were taken for the PGM samples at concentrations, the linear viscoelastic regime (LVR) was determined for each concentration solution; this is an important step to determine the range in which the storage modulus ( $G'$ ) and the loss modulus ( $G''$ ) are independent of stress amplitude ( $\sigma_0$ ). This was done by performing a dynamic stress sweep to observe how the material responds to increasing deformation at a constant frequency and temperature. For the LVR experiment, a constant frequency of 1 rad/s was selected over a stress range of 0.01 to 100 Pa at 25 °C. The LVR was determined by choosing the average strain value that produces constant elastic moduli variable. Frequency sweep oscillation experiments were carried out on the 1, 2 and 5 wt% mucin solutions at each samples strain value related to the LVR

results at 25 °C and 37 °C over a 0.01 to 100 rad/s frequency range. All error bars and values for data shown are 95% confidence intervals.

Dynamic Light Scattering. DLS particle sizing was performed using a NanoBrook Omni PALS instrument equipped with Brookhaven Instruments Particle Solutions Software. This equipment was used to perform particle sizing of the PGM samples at 1, 2 and 5 wt%. When running DLS particle sizing, sample must be transparent to allow the laser beams pass through to interact with the particles. To prepare samples, 1:100 dilutions were performed by method of serial dilution before running the experiments. Following the serial dilution of the 1, 2, and 5 wt% PGM samples, the final concentrations were 0.01, 0.02 and 0.05 wt% respectively. Experiments were conducted using a 90-degree laser angle, and a 640nm laser wavelength. All error for data is shown as 95% confidence intervals.

Zeta Potential. Zeta potential experiments were performed using a Brookhaven Instruments NanoBrook Omni phase analysis light scattering (PALS) instrument. This equipment was used to assess the surface charge while varying the pH of the PGM samples. To prepare samples for this experiment, 1:100 dilutions were performed by method of serial dilution before running the experiments. Following the serial dilution of the 1, 2, and 5 wt% PGM samples, the final concentrations were 0.01, 0.02, and 0.05 wt%, respectively. The samples at different pH values were prepared discretely using buffers before running the experiment. Buffers used were 0.1 M and 0.1 mM nitric acid and 0.1 M and 0.1 mM potassium hydroxide. Experiments were conducted at a 640 nm laser wavelength. All error for data is shown as 95% confidence intervals.

#### *2.4. Results and Discussion*

Several experiments were conducted to study the effects of temperature, concentration, and pH on PGM. Surface tension measurements were collected under these conditions to see how changes in the microstructure change affect the surface tension of PGM. Microstructural and network changes in mucin also affects the sol-gel transition of the samples, and so rheology data was collected to take a closer look at these changes. Zeta potential was used to understand the charge state of PGM molecules to explain its macroscopic properties and dynamic light scattering was used to study how the size of the particles changed with under different pH conditions. Zeta potential and

dynamic light scattering pH studies<sup>16</sup> have shown that particle size depends on the zeta potential and pH of the solution as maximum aggregation is seen to occur at the isoelectric point where the samples has a net charge of zero.

### *2.5. PGM Temperature and Concentration Studies*

Surface tension is a very sensitive parameter that can detect even the smallest of changes at the molecular level. Taking the chemical structure into account, the properties of mucin are dependent on the properties of the contact environment. Factors such as temperature and acidity might provide a disturbance in the chemical structure of mucin and eventually change its properties.<sup>17</sup> The characterization of the surface properties of mucin are key to understanding how these biopolymers change under different pH and temperature conditions. Surface tension data is also of great importance in biomaterial applications.

To determine the feasibility and accuracy of the surface tension measurements, solvents of different surface tensions were chosen and their surface tension data was collected and compared to literature values. The rationale for conducting these experiments was to develop a straightforward and reproducible way to evaluate the surface properties of PGM so that its characteristics can be studied. The model solvents used for this study are Nanopure<sup>TM</sup> water, hexadecane and pyridine. These were chosen because of the availability of surface tension data in literature.

In comparison to literature values, the surface tension values of Nanopure<sup>TM</sup> water, mucin and pyridine at room temperature (25 °C) are shown to have less than 10% difference. These results confirmed that the pendant drop method of measuring surface tension is capable of analyzing all types of solvents and was an appropriate method to detect microstructural changes in for our PGM experiments. The results and percent difference calculations are shown below in Table 1 below. Following the surface tension experiments on the solvents, it was determined that surface tension measurements, using pendant drop is a very sensitive way of measuring changes in the microstructure of samples. The surface tensions of 1, 2 and 5 wt% PGM samples were measured at 25°C and 37°C using the same process and the results are shown in Figure 1 below.

**Table 1:** Surface tension values of model liquids shows very little deviation between our experimental SFT measurements and literature values.

Solvent	Dispersion ( $\delta_d$ ) <sup>18</sup>	Polar ( $\delta_p$ ) <sup>18</sup>	Hydrogen Bonding ( $\delta_h$ ) <sup>18</sup>	Experimental SFT [mN/m]	Literature SFT [mN/m] <sup>19</sup>	% Difference
Hexadecane (C <sub>16</sub> H <sub>34</sub> )	16.3	0	0	28.85	27.47	4.90
Pyridine (C <sub>5</sub> H <sub>5</sub> N)	19.0	8.8	5.9	34.60	38.00	9.37
Nanopure™ water (H <sub>2</sub> O)	15.5	16.0	42.3	73.79	72.80	1.35

**Table 2:** Aqueous PGM solutions surface tension was found to decrease with PGM concentration and temperature. A wait time of 30 seconds was observed to allow drops stabilize before collecting surface tension measurements.

PGM wt%	PGM Surface Tension at 25°C [mN/m]	PGM Surface Tension at 37°C [mN/m]
1	68.36	66.55
2	67.54	64.31
5	62.95	62.11



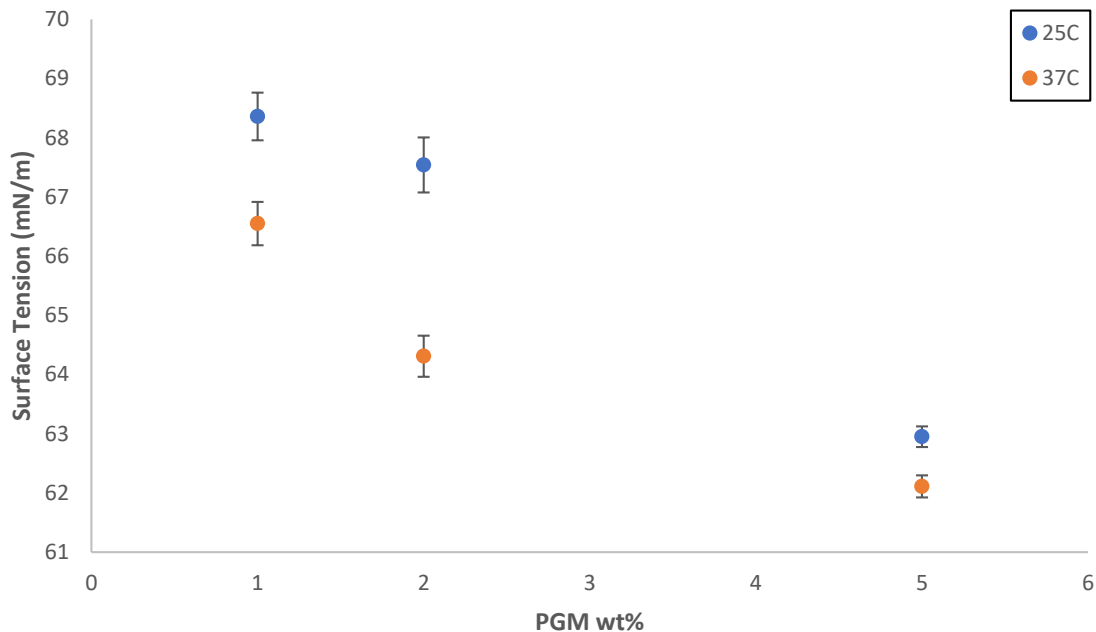


**Figure 1:** Surface tension of PGM solutions decreases with increasing PGM concentration and a shift from room temperature (25 °C) to physiological temperature (37 °C).

It was observed that the overall surface tension decreased with increasing concentration of PGM regardless of temperatures. This trend occurs as a result of the stronger inter-molecular forces brought about by hydrogen bonding in lower concentrations of PGM. An increase in the concentration of a PGM means there is a decrease in the amount of water in the solution and thus less hydrogen bonding and weaker intermolecular forces. Surface tension depends heavily on the intermolecular forces present and increases with increasing strength of intermolecular forces.<sup>20</sup> Polymer-polymer interaction in the solutions of different concentrations also plays an integral role in the trend observed in Figure 1 above.

In more concentrated PGM solutions with less water, polymers are more likely to interact with themselves whereas in a more dilute solution, the polymers will have more interaction with H<sub>2</sub>O molecules. Therefore, as the concentration of the PGM solutions are increased there is more polymer-polymer interaction and this causes the chains to get more entangled. In sufficiently dilute solutions such as the 1 wt% sample, polymer chains are disengaged, separated, and behave as

individual hydrodynamic unit, however polymer chains are more entangled in solutions of polymers of sufficiently high concentration.<sup>21</sup>

Comparing the surface tension values at the studied temperatures, it was observed that the surface tension for PGM samples at 37 °C are lower than those at 25 °C. This behavior is expected because surface tension is highly dependent on the intermolecular forces. At higher temperatures, the PGM molecules become more active and move faster. This causes the water forces to be more unstable and lowers the surface tension of the solution.

To further study the extent of the entanglement and the sol-gel transition of PGM, a rheology study was carried out. Rheology is a suitable technique for the investigation of PGM because mucin is a viscoelastic gel (exhibits both liquid and solid characteristics).<sup>22</sup> Stress sweep experiments were conducted to determine the linear viscoelastic region (LVR) of PGM samples at different concentrations and temperatures. The LVR information gives frequency sweep operating range where the storage modulus ( $G'$ ) and the loss modulus ( $G''$ ) are independent of stress amplitude ( $\sigma_0$ ). LVR data can be found in Appendix C.

Following the LVR experiments, frequency sweep experiments were carried out at 25 °C and 37 °C over a 0.01 to 100 rad/s frequency range. Strain amplitude value gotten from LVR experiments was  $10^{-2}$  Pa for 1, 2, and 5 wt% PGM solutions at 25 °C and 37 °C. This was done to examine the viscoelastic behavior of PGM. Rheology data are presented separately for the 1, 2, and 5 wt% PGM solutions in Fig. 2-4. Figures 5-6 provide an overlay of these data sets.

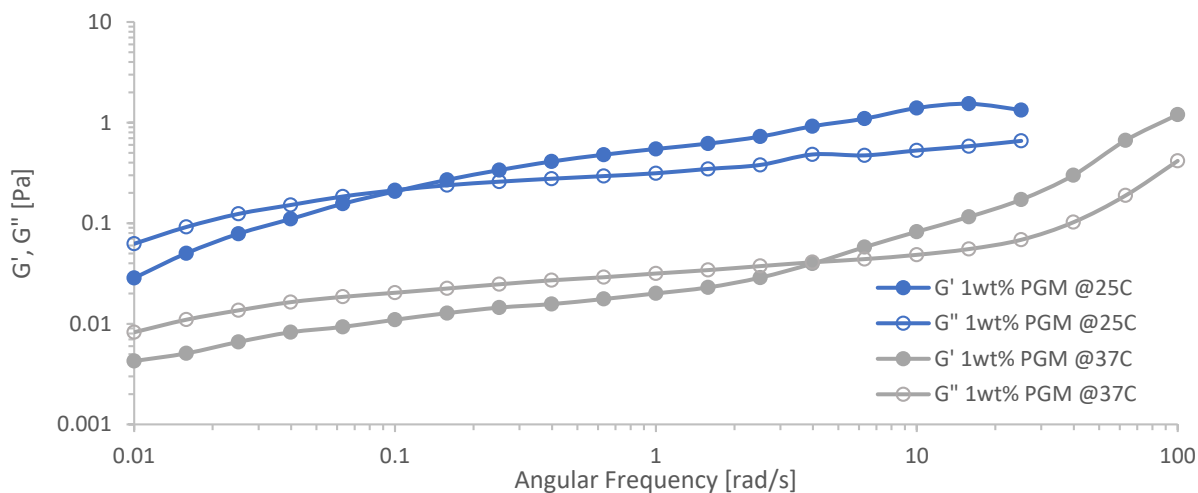


**Figure 2:** Storage and loss modulus increase for 1wt% PGM at 25 °C. The sol-gel transition also occurs at a lower frequency for the 1 wt% PGM solution at 25 °C

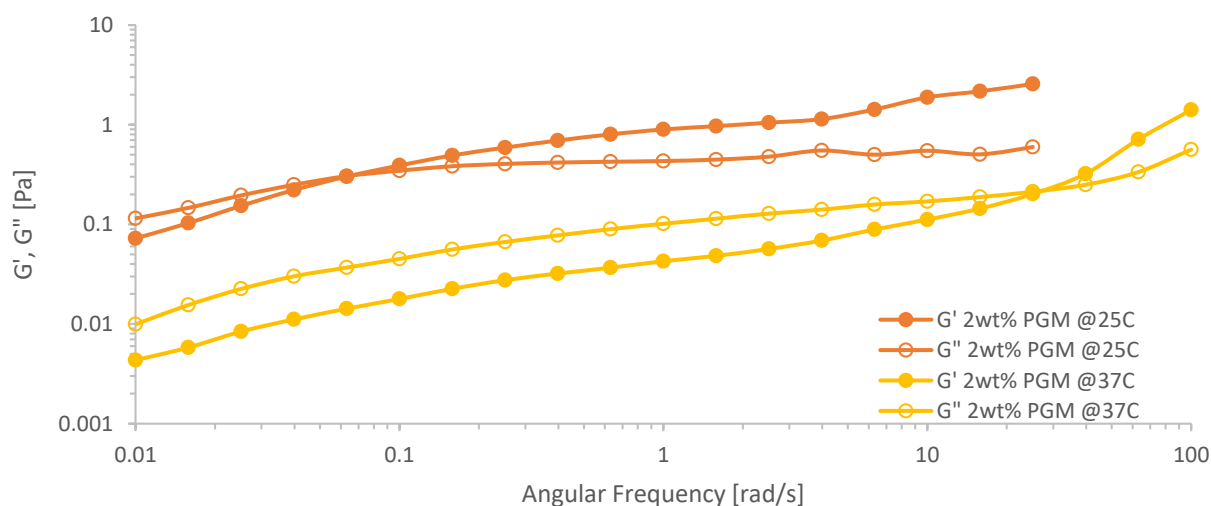


**Figure 3:** At 25 °C both the storage and loss moduli for 2 wt% PGM are higher than at 37 °C . The sol-gel transition occurs at a lower frequency for 2 wt% PGM at 25 °C—than at the physiological temperature of 37 °C.

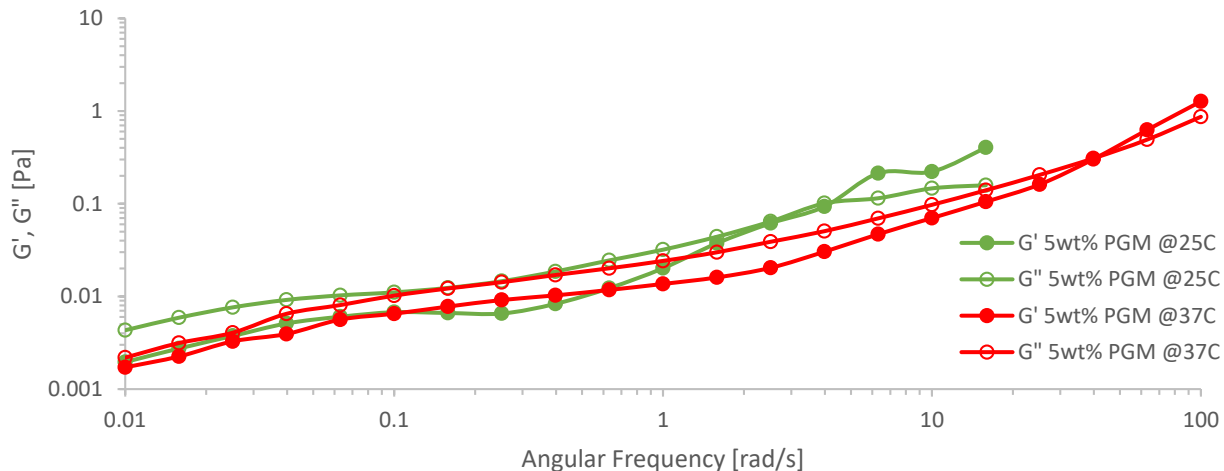


**Figure 4:** Storage and loss modulus are shown to overlap for 5 wt% PGM at 25 °C and 37 °C. Sol-gel transition occurs at lower frequency for 5 wt% PGM at 25°C

For results shown in Figures 2-4, it is observed that the storage modulus ( $G'$ ) and the loss modulus ( $G''$ ) increased as a function of frequency similar to the study conducted by Hamed et al.<sup>23</sup> When the storage modulus  $G'$  is dominant over the loss modulus  $G''$  it indicates a gel-like material response and a sol-gel transition occurs, and when the loss modulus  $G''$  is dominant over the storage modulus a liquid-like response is observed.<sup>24</sup> When the sol-gel transition occurs, the viscosity becomes infinite and the network in the gel provides resistance to elastic deformations.<sup>2</sup> On the basis of this criterion it is clear that increasing the temperature of PGM solutions keeps the solutions in a liquid-like state for much longer than it would at room temperature. This happens because an increase in temperature causes the molecules to vibrate and disrupt the bonds therefore it takes longer to stabilize and undergo the sol-gel transition.

Frequency sweeps of PGM solutions shows evidence of a dramatic change in the sol-gel transition (crossover) points of PGM solutions at 25 °C and 37 °C. The sol-gel transition occurs at a lower angular frequency for 25 °C and a higher value for the 37 °C. We also see that the transition occurs at higher force values with the exception of 5 wt%. This is likely due to the fact that PGM at 5 wt% is much thicker and viscous than 1 and 2 wt% solutions. As a result of this, physical entanglements are created and broken quickly compared to the rate of deformation, thus less force is required for the sol-gel transition to occur.<sup>25,26</sup> The 5 wt% PGM transitions occurred at a higher frequencies compared to 1 and 2 wt% for both at 25 °C and 37 °C indicating an entanglement network system.<sup>27</sup> The decrease in surface tension and higher frequency observed in 5wt% PGM samples are needed to induce sol-gel transition.

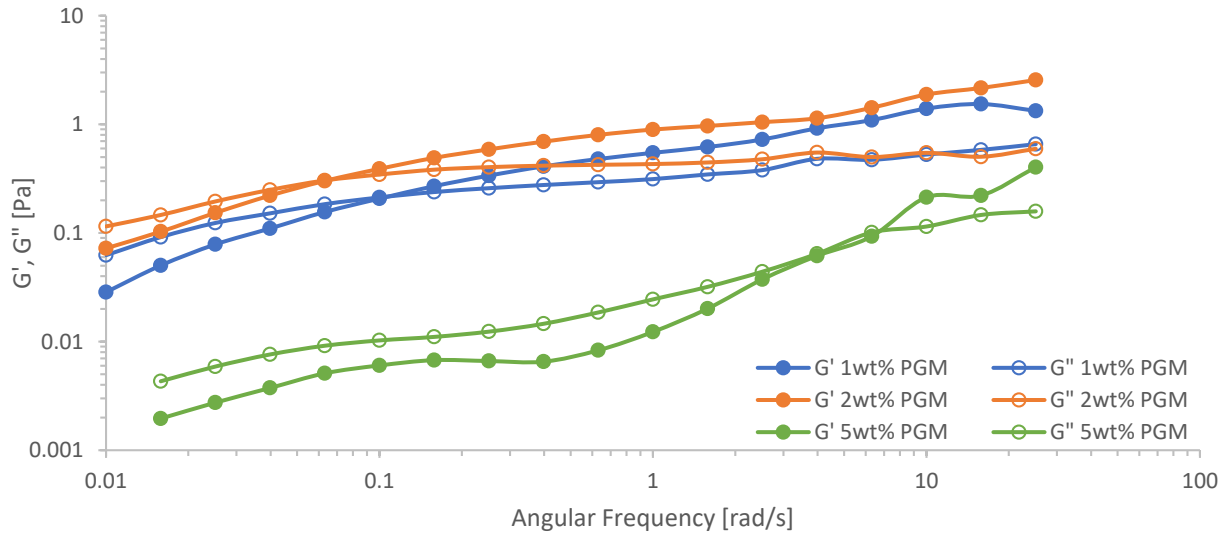


**Figure 5:** Storage and loss modulus values for 1 wt% and 2 wt% PGM samples are significantly higher than those for 5 wt% at 25°C. The sol-gel transitions are observed at 0.06-0.1 rad/s for 1 and 2 wt% PGM and at ca. 4-5 rad/s for the 5 wt% PGM sample.

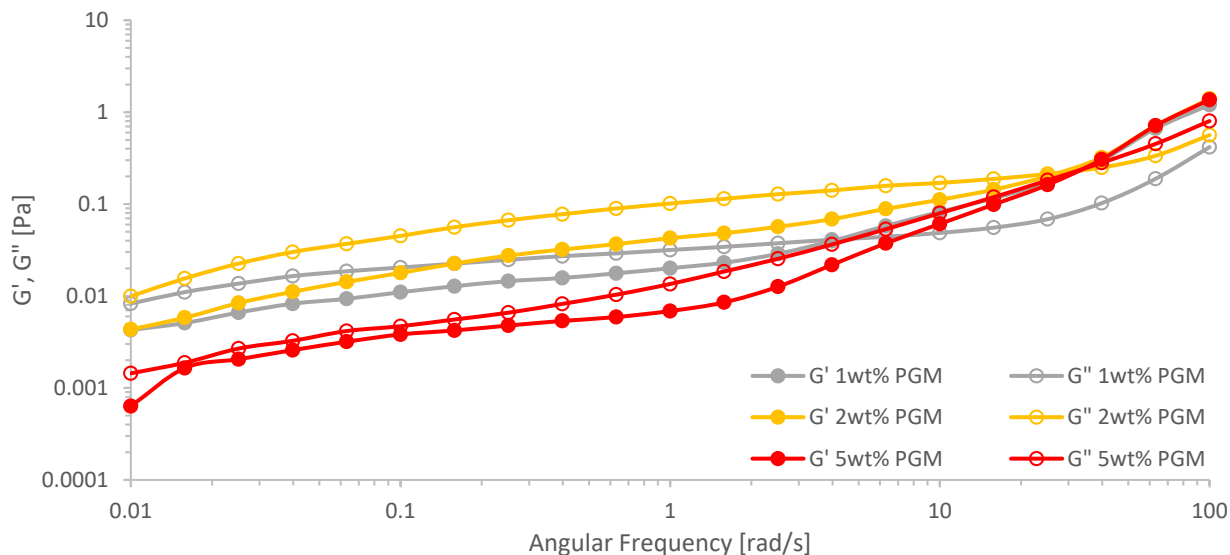


**Figure 6:** Frequency sweep data for PGM solutions at 37 °C showing the sol-gel transition at a much higher value, approx. 35 rad/s, than was observed for the 25 °C data.

To study the particle sizing and aggregation of PGM at different concentrations dynamic light scattering (DLS) experiments were conducted. The results shown in Figure 7 below show a decrease in the mean diameter by number as the concentration of PGM is increased and an increase in mean diameter at 37 °C. Increasing the temperature of PGM increases the kinetic energy of the PGM molecules causing the particles to interact more with one another and aggregate.

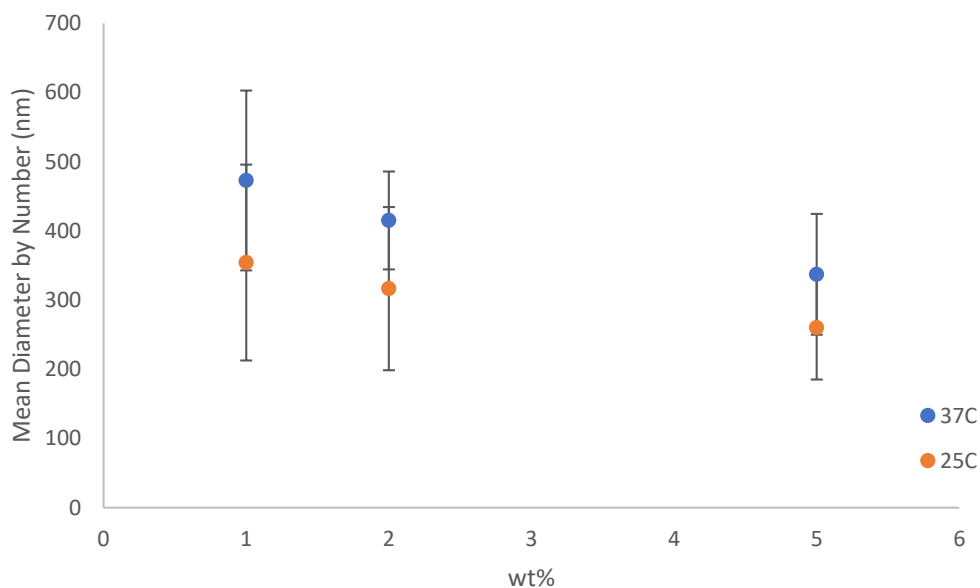


**Figure 7:** PGM mean diameter by number decreases with increasing PGM concentration and tends towards aggregation when the temperature is increased to 37 °C.

## 2.6. PGM pH Studies

A pH study was conducted on PGM samples by varying the pH and conducting surface tension, particle sizing and zeta potential experiments. The pH values of the solutions were varied using 0.01 M nitric acid (HNO<sub>3</sub>) and 0.01 M sodium hydroxide (NaOH). Native mucin has a pH of 4.699 and Figures 8 to 10 show surface tension results between pH values of 3-8 at 25 °C. There is an overall downward trend in the surface tension as the pH of the solutions increase. Studies conducted<sup>4, 11, 24, 28</sup> have shown that lowering the pH of PGM causes a sol-gel transition to occur and this leads to changes in the polymer network structure of the mucin. Sol-gel transitions have

been shown to take place in mucin due to environmental factors such as pH, ion concentration, inclusion/particle chemistry and size, temperature, and shear forces.<sup>11</sup>

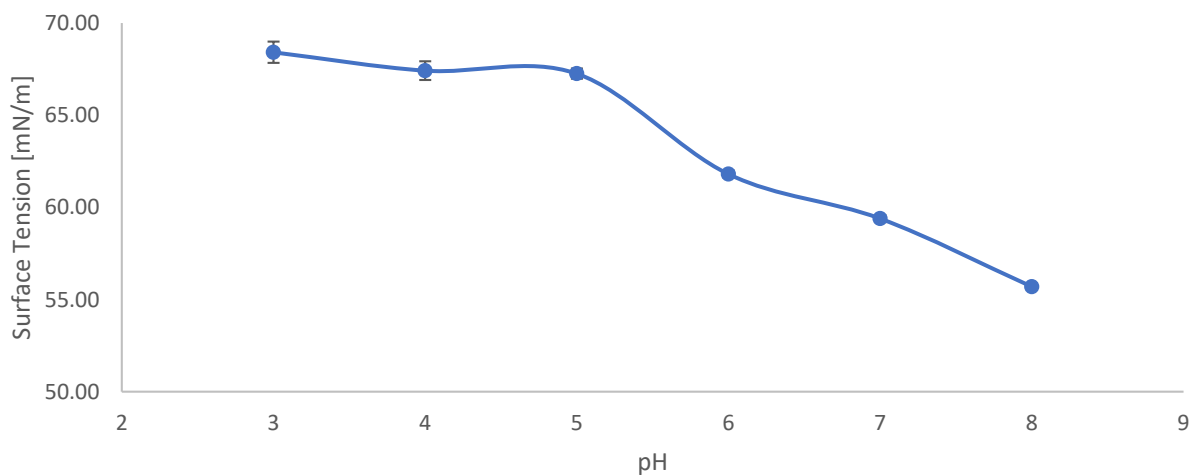


**Figure 8:** Surface tension decreases as pH increases in the 1 wt% PGM sample with a steep inflection between pH 5-6.

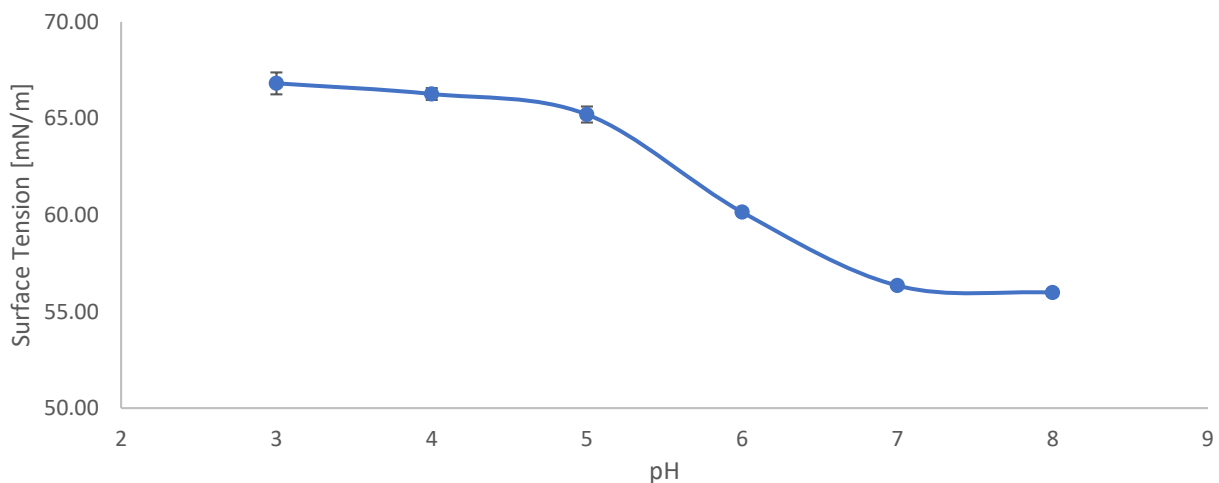


**Figure 9:** Surface tension decreases as a function of pH for 2wt% PGM solution; this trend matches the 1 wt% sample showing an inflection between pH 5-6.



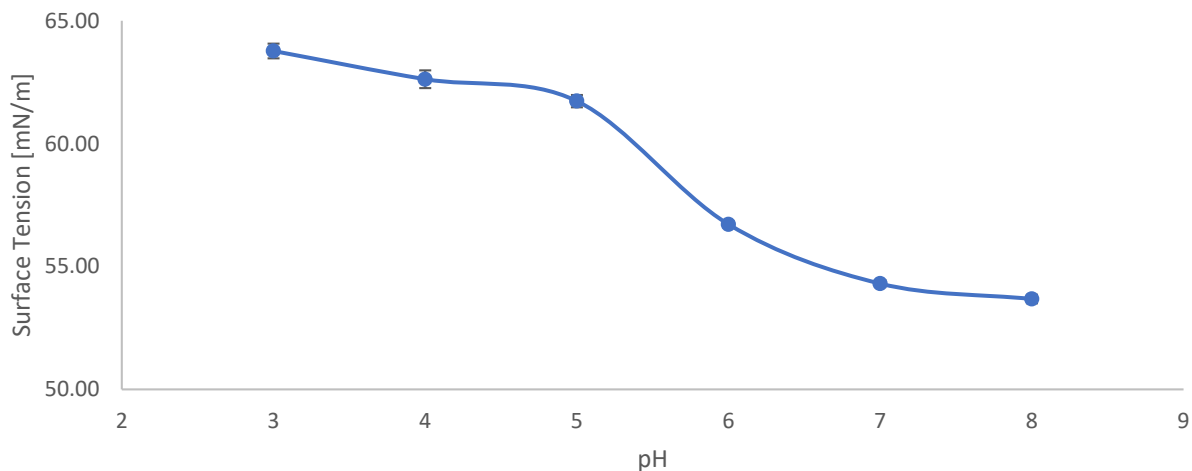


**Figure 10:** Surface tension values for the 5 wt% PGM sample are shifted down for pH values < 7 in comparison to the 1 and 2 wt% samples. The same downward trend and inflection between pH 5-6 is also observed for PGM surface tension at 5 wt%.

Atomic force microscopy and rheology experiments on gastric mucin have revealed aggregation at low pH.<sup>11, 29, 30</sup> Aggregation of mucin samples cause the lower pH samples to have strong effects on the network structure of the mucin which in turn affects the surface tension values. Studies have shown that at lower pH values, the contracted chains build up a network with weak connectivity and strongly heterogeneous networks of entangled chains are formed<sup>31</sup> causing higher surface tension values. The surface tension at higher pH values significantly decrease especially between pH values of 5 and 6. Under these conditions, a homogeneous network with

evenly spread out chains are observed.<sup>31</sup> A schematic illustration of the network structures observed at different values of pH is displayed in Figure 11.

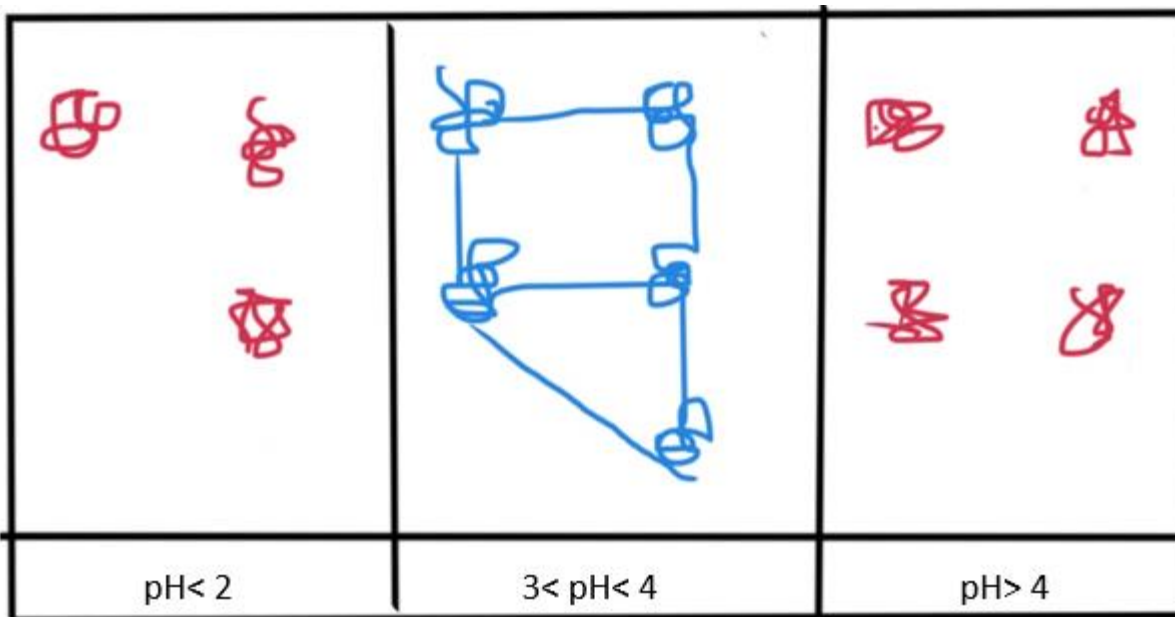


**Figure 11:** Illustration of network formation in PGM at different pH values. Constricted chains observed under very acidic conditions and network structure seen at higher pH. Adapted from ref [31].

To further study how the change in the mucin network structure affects its properties, zeta potential (ZP) and dynamic light scattering (DLS) experiments were conducted. These experiments study the changes in the net surface charge and particle size of PGM. The magnitude of electrostatic interactions between charged surfaces was studied by running zeta potential experiments on PGM samples with varying pH and concentrations. Varying the pH value of the aqueous phase influences two mechanisms: functional group dissociation and ion adsorption. In addition to the solution pH, the concentration and type of salt present in the solution affects the ionic state of the biomolecules.<sup>32</sup> In Figure 12 below, we notice that PGM is negatively charged at pH values greater than 3 and the charge density increases progressively with rising pH, leading to more extended chains due to enhanced electrostatic repulsions.<sup>31</sup> At low pH, biomolecules

generally presented positive zeta potentials which decreased when pH was raised<sup>32</sup> and a similar trend is observed in Figure 12.

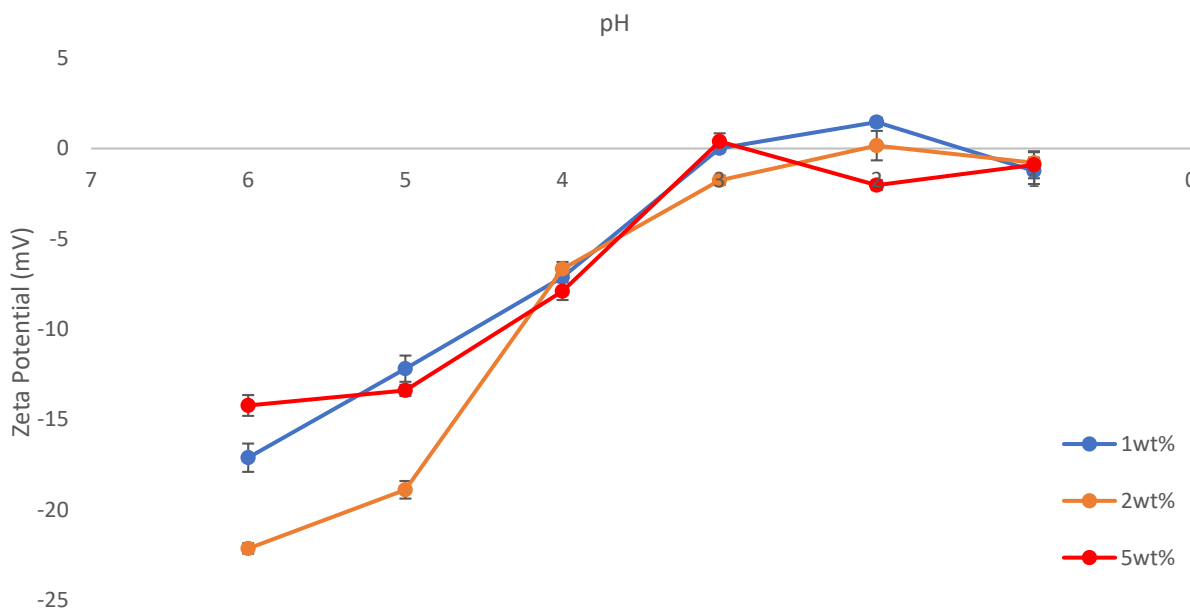


**Figure 12:** PGM zeta potential as a function of pH. At pH values  $\geq 5$ , the PGM samples are significantly electronegative and the PGM strands should another and remain stable in solution. At lower pH, the zeta potential decreases approaching the isoelectric point. The PGM samples show that charge-related aggregation is likely under very acidic conditions ( $\text{pH} \leq 4$ ) and aggregation is expected to occur under these conditions.

A point of interest in this experiment in this experiment is the isoelectric point (IEP). The IEP is the pH of a solution at which the net charge or zeta potential of protein is zero.<sup>32</sup> At the IEP, the PGM structure is more hydrophobic, more compact and less stable due to absence of inter-particle repulsive forces thus making it easier for particles to aggregate and precipitate.<sup>32-34</sup> The IEP of the 1, 2 and 5wt% PGM solutions shown vary and this is caused by different ionic environment such as ionic strength, pH and ion type.<sup>32</sup> The trend above the isoelectric point was surprising. We anticipated that at very low pH there would be very little impact on the surface charge of the particles, however, the surface charge began to decrease. This is likely due to a strong association of the mucin with  $\text{H}^+$  ions at low pH.

We further studied the effect of pH on the size of PGM aggregates. We hypothesized that the nature of the charge of PGM observed in Figure 12 would play an important role in the size of the particles. To investigate this further, we studied changes in diameter of the mucin with changes in pH of the solution using DLS. It was observed that the size of the particles is significantly smaller at pH values higher and lower than the isoelectric points of the respective concentrations.

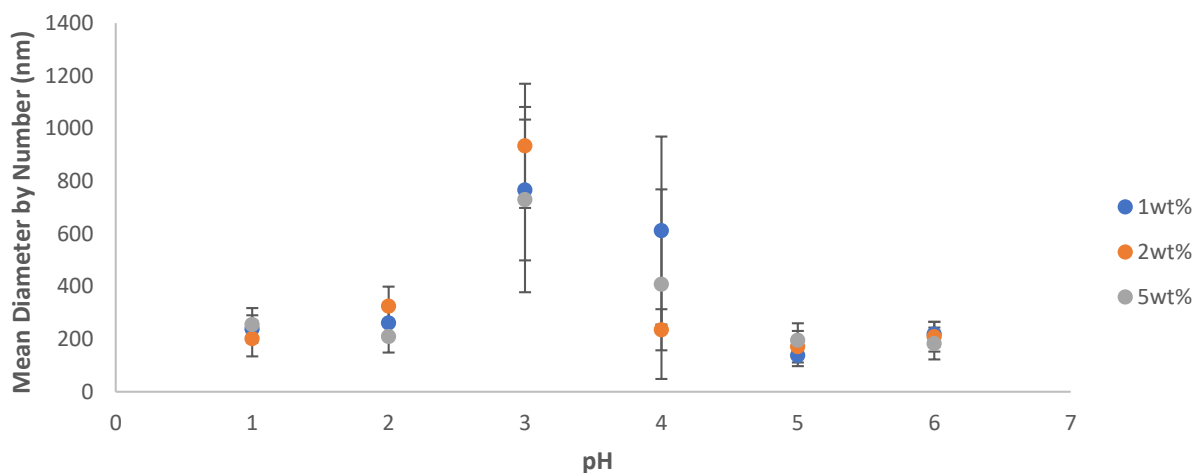


**Figure 13.** DLS results show maximum aggregation of PGM molecules observed at the onset of the isoelectric point region (pH 3-4) for the 1, 2, and 5 wt% PGM samples.

DLS results shown in Figure 13 show that the maximum diameter occurs at pH 3 (isoelectric point) and this suggests that aggregation, gelation, and the formation of intertwined chains are promoted under these conditions. This is likely due to high density of charge in the samples with pH lower and higher than the isoelectric point which exhibits electrostatic repulsions between the polymer chains at the microscopic level, leading to the formation of smaller aggregates. On the other hand, as we reach the isoelectric point, the reduced electrostatic repulsions result in the formation of larger aggregates.<sup>16</sup> A comparison of the DLS and ZP results are shown in Figure 14 and this indeed proves that there is a direct relation between surface charge and particle size. A sol-gel transition map showing the effect of pH on the state of PGM considering the surface tension, DLS, and ZP data can be found in Figure 43 in Appendix C.

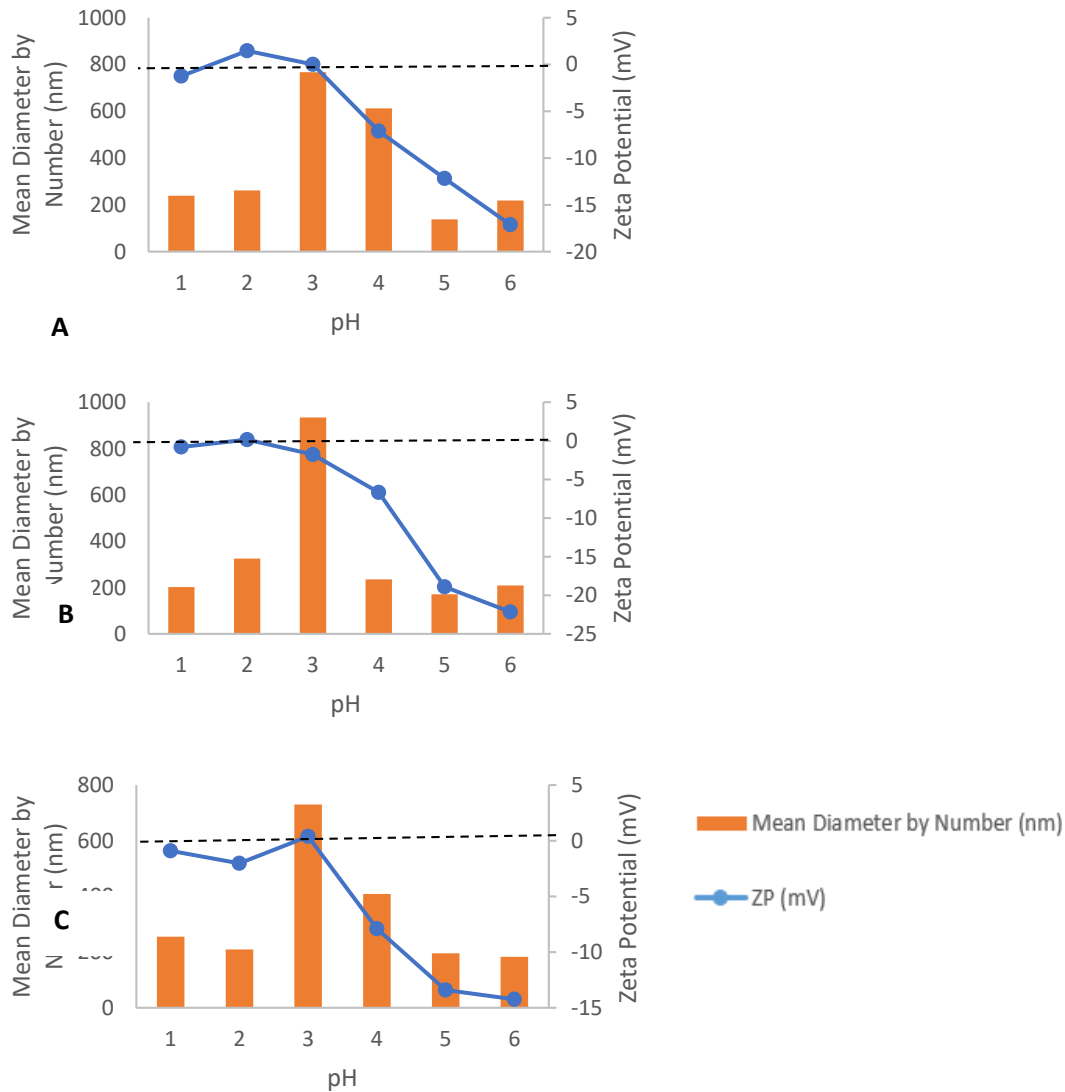


**Figure 14:** DLS and ZP results show decrease in diameter at pH lower and higher than the isoelectric point for PGM solutions at (A) 1 wt%, (B) 2 wt%, and (C) 5 wt%.

### 2.7. Conclusions

This study confirms that microstructural changes in PGM occur in response to changes in concentration, temperature, and pH. Nano- and micro-structural changes have been examined

using surface tension, rheology, dynamic light scattering, and zeta potential experiments. Temperature and concentration studies show that the surface tension and mean diameter by number decrease with increase in concentration, however polymer-polymer interaction increases at elevated temperatures causing aggregation and leading to larger particle sizes. Rheology studies also show that PGM higher frequencies are needed to achieve sol-gel transition at elevated temperatures. Conducting pH studies show direct relationship between dynamic light scattering and zeta potential proving that surface charge greatly affects the aggregation of PGM and the isoelectric point supports gelation which induces polymer-polymer interaction that causes particles to aggregate. Surface tension experiments revealed higher surface tension values when a more constricted network structure is present under acidic conditions. In future work, a more in-depth examination of the relationship between pH and temperature for PGM would be interesting especially as the structure of gastric mucin controls drug and nutrient uptake in the digestive system and the pH and temperature vary significantly under physiological and pathological conditions.

## Chapter 3. Effect of Silica Nanoparticle Addition on Mucin Microstructure

### 3.1. Abstract

In this work, silica nanoparticles (SiNPs) synthesized using the Stöber method were integrated into aqueous porcine gastric mucin (PGM) and studied at different concentrations. The synthesis method is described and samples were characterized using SEM, static surface tension, rheology, FT-IR, zeta potential, and dynamic light scattering. Zeta potential and dynamic light scattering revealed that with increased addition of nanoparticles, the surface charge decreased and approached the isoelectric point which induced aggregation in PGM samples. Frequency sweep data shows that a gel-like material response is maintained when SiNPs are incorporated into PGM samples.

### 3.2. Introduction

Mucus is a viscoelastic, complex fluid that coats the surfaces of the gastrointestinal, urogenital, and respiratory tracts, as well as the ocular surface. It is critical to the hydration of these surfaces and their protection from contact with environmental irritants. Mucus is mainly water (90-95% w/w) with approximately 1% w/v electrolytes.<sup>35</sup> Mucins are high-molecular weight glycoproteins, which consist of a protein core and feathering polysaccharide side chains (Figure 15). When mucins are hydrated in water, the mucins swell and can physically entangle with each other. Mucins also participate in primary and secondary inter-polymer and intra-polymer chemical bonding. The physical and chemical interactions among mucins establish a cross-linked mucin network which gives rise to the viscoelastic behavior of mucus.<sup>35</sup>

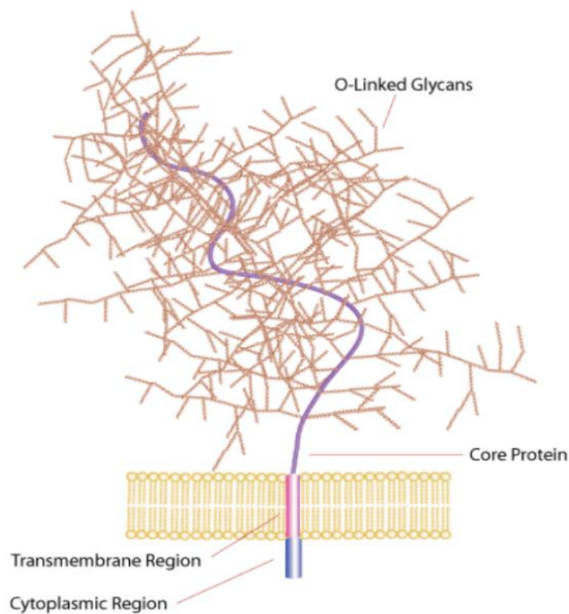


**Figure 15:** Schematic representation of a bound (transmembrane) mucin. This study uses porcine gastric mucin, which contains mainly secreted mucins collected from the gastric epithelium. [Image Source: Sigma-Aldrich, *Mucin*]

The mucin network is selectively permeable to particles of specific (i) sizes and (ii) chemistries. (i) Non-mucoadhesive particles are involved in length-scale-dependent interactions with mucus that influence the mucus' microrheological behavior. This interactive length-scale depends on the type of mucus and is usually between tens of nanometers to microns.<sup>36</sup> Mucoadhesive compounds or polymers are chemically attracted to reactive sites on mucins. Chitosan is a well-known mucoadhesive polymer with alcohol and amine groups that bond to charged groups on the polysaccharide chains of mucin.<sup>37</sup> Coupled together, NPs functionalized with mucoadhesive compounds are of interest as a drug delivery system. NPs can be loaded with drugs, and the mucoadhesive surface draws the NPs to a mucosal surface where the drugs can be released<sup>38</sup>.

The goal of this research is to determine the rheological, surface tension, and structural effects of the doping concentration of unfunctionalized silica NPs on aqueous mucin solutions. This research will establish a baseline to build future studies about the rheological effects of



functionalized, mucoadhesive NPs in mucin solutions. SiNP concentrations of 2, 1, 0.5, 0.3, and 0.1 mg/mL in 1% w/w mucin solutions were studied. The SiNP concentrations used fell within the range of NP concentrations used in previous studies on mucus.<sup>39, 40</sup> Fourier transform infrared spectroscopy (FTIR), surface tension pendant drop, dynamic light scattering particle sizing (DLS), zeta potential Phase Analysis Light Scattering (PALS), and rheometer frequency sweeps were used to characterize the mucin solutions.

### 3.3. Materials and Methods

Silica Nanoparticles. Uniform, monodisperse, SiNPs were synthesized using the Stöber process as shown in Figure 16. For this study, 100 mL ethyl alcohol (EtOH, 200 proof, anhydrous,  $\geq 99.5\%$ , Sigma-Aldrich), 6 mL ammonium hydroxide (NH<sub>4</sub>OH, ACS reagent grade, 28-30%, VWR), and 8 mL tetraorthosilicate (TEOS, 98%, Sigma-Aldrich) were reacted in a well-stirred round-bottom flask for 24 hours.

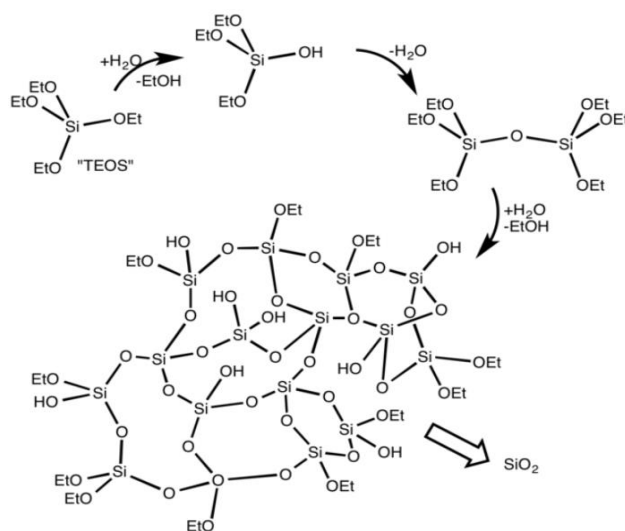


**Figure 16:** One-step base-catalyzed Stöber process synthesis mechanism. First, an ethoxy group on a tetraorthosilicate molecule is cleaved via hydrolysis. Immediately, the newly formed ethoxysilanol joins another silanol via the condensation reaction. Ammonium hydroxide acts as a catalyst in the hydrolysis reaction. [Image Source: Wikimedia Commons, *Sol-Gel-Cartoon*]

The reaction mixture was completely dried using a rotary evaporator, and the NPs were resuspended in 20 mL Nanopure™ water and sonicated for 30 minutes. Unreacted TEOS was

removed from the NPs via Spectrum™ Spectra/Por™ 1 RC dialysis membrane tubing (6000-8000 Dalton MWCO). The NP-water solution was loaded into the dialysis tubing and placed in a Nanopure™ water bath with a volume ratio of 1:100 (NP solution: water bath). The water bath was heated to 40°C and stirred moderately with a magnetic stir bar (<100 rpm). The water bath was replaced after 1, 3, 6, and 20 hours to maintain the concentration driving gradient.

After processing with the dialysis membrane, the NP solution was completely dried in a drying oven at 70°C. The dried NPs were massed and resuspended in Nanopure™ water to a NP concentration of 10 mg/mL. The stock NP solution was sonicated for 30 minutes to return the NPs to their original uniform, monodisperse state. Diluted NP solutions (~0.05 mg/mL) were prepared in isopropyl alcohol and Nanopure™ water to be used in baseline characterization with FTIR and DLS, respectively.

The morphology of the SiNPs were examined using scanning electron microscopy (SEM). Figure 17 shows images of the synthesized 75nm SiO<sub>2</sub>. Samples were taken from the reaction mixture and dried on a wafer before imaging. Nano spheres are spherical, monodispersed and no visible pores are observed. Some agglomeration is observed in the particles.

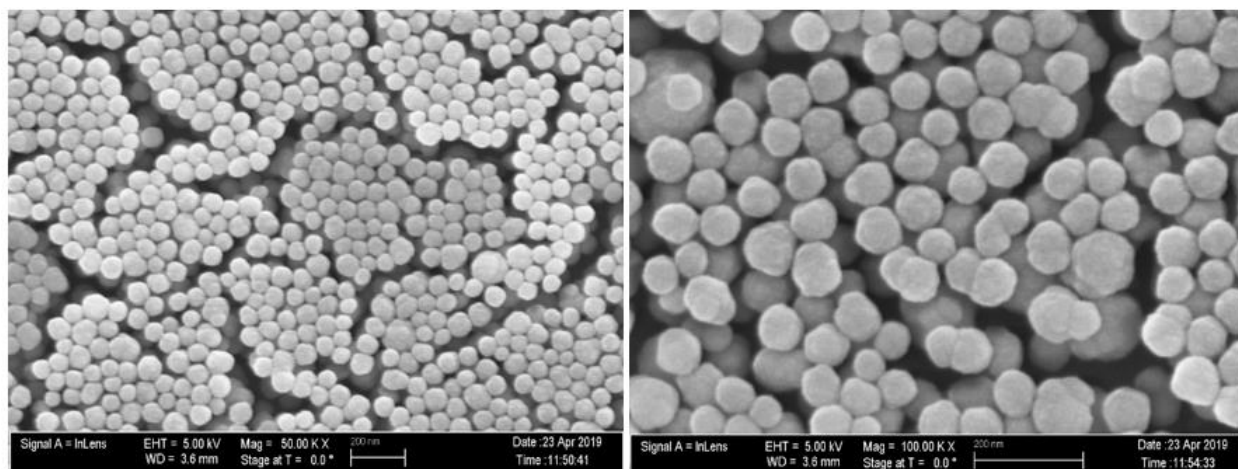


**Figure 17:** SEM micrographs of Stöber process-synthesized silica nanoparticles indicate particle diameter around 70 nm. The batch of nanoparticles scanned here were not the same batch used to prepare the mucin solutions; however, both batches were synthesized using the same ratios of chemicals and the same reaction conditions.

Preparation of blank and silica nanoparticle-doped mucin solutions. Rehydrated mucin is used in this study as it is comparable structurally to native mucus and readily available. A blank mucin 10 mg/mL (1 wt%) solution was prepared with lyophilized Mucin from Porcine Stomach Type II from Sigma-Aldrich (PGM) and Nanopure™ water. The blank mucin solution was used as a control and reference for the silica NP-doped mucin solutions. The stock silica NP solution was diluted with Nanopure™ water to 2, 1, 0.5, 0.3, and 0.1 mg/mL, and PGM was added to each NP solution to make 1% w/w mucin solutions. To ensure thorough hydration of the mucins, all mucin solutions were sonicated for 30 minutes and refrigerated for 24 hours before experiments were run. All experiments were conducted at room temperature.

The blank mucin solution was used as a control and reference for the silica NP-doped mucin solutions. The stock silica NP solution was diluted with Nanopure™ water to 2, 1, 0.5, 0.3, and 0.1 mg/mL, and PGM was added to each NP solution to make 1% w/w mucin solutions. To ensure thorough hydration of the mucins, all mucin solutions were sonicated for 30 minutes and refrigerated for 24 hours before experiments were run. All experiments were conducted at room temperature.

Pendant Drop. Surface tension measurements at room temperature were collected using a Krüss Drop Shape Analyzer-DSA25. This was used to measure the surface tension of PGM + SiNPs. SiNPs were made to 2, 1, 0.5, 0.3 and 0.1 mg/mL concentrations and 10 mg/mL of PGM was added to the solutions. After drops were dispensed, a wait time of 30 seconds was observed before collecting data. All error for data is shown as 95% confidence intervals.

Fourier Transforming Infrared Spectroscopy (FTIR). Physical characterization of mucin bound SiNPs was confirmed using FTIR spectroscopy. Spectral data was acquired using a Thermo Fisher Nicolet iS50 instrument with a deuterated triglycine sulfate (DTGS) detector, attenuated total reflectance (ATR) accessory with diamond-ZnSe crystal and a XT-KBr beam splitter. Nanoparticles in isopropyl alcohol and NP: PGM solutions were drop-cast onto the ATR crystal for measurements at ambient temperature (approximately 23 °C).

Rheology. Rheological measurements were collected using a TA instruments Discovery Hybrid Rheometer II using Trios software (v5.00). A 40 mm cone with an angle of 2.013° was used to perform frequency and flow sweeps on the solutions containing SiNP+ PGM solutions. The angled 40 mm geometry was chosen because the diameter was appropriate for samples with medium viscosity and the cone shape produces a smaller gap height closer to inside so the shear on the sample is constant.<sup>15</sup>

Before rheological measurements were taken for the samples, the linear viscoelastic regime (LVR) was determined for each concentration solution; this is an important step to determine the range in which the storage modulus ( $G'$ ) and the loss modulus ( $G''$ ) are independent of stress amplitude ( $\sigma_0$ ). This was done by performing a dynamic stress sweep to observe how the material responds to increasing deformation at a constant frequency and temperature. For the LVR experiment, a constant frequency of 1 rad/s was selected over a stress range of 0.01 to 100 Pa at 25 °C. The LVR was determined by choosing the average strain value that produces constant elastic moduli variable.

Frequency sweep oscillation experiments were carried out on the 1, 2 and 5 wt% mucin solutions at each samples strain value related to the LVR results at 25 °C and 37 °C. over a 0.01 to 100 rad/s range. All error for data is shown as 95% confidence intervals.

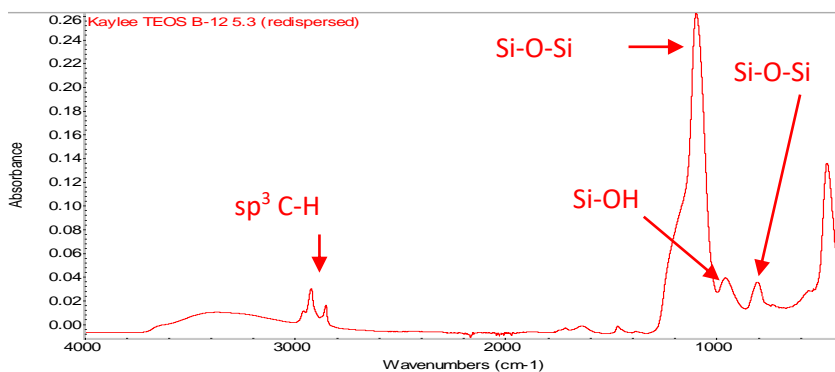
Dynamic Light Scattering. DLS particle sizing was performed using a NanoBrook Omni PALS instrument equipped with Brookhaven Instruments Particle Solutions Software. This equipment was used to perform particle sizing of the PGM + SiNP solutions. When running DLS particle sizing, sample must be transparent to allow the laser beams pass through to interact with the particles. To prepare samples, 1:100 dilutions were performed by method of serial dilution before running the experiments. Experiments were conducted using a 90-degree laser angle, and a 640nm laser wavelength. All error for data is shown as 95% confidence intervals.

Zeta Potential. Zeta potential experiments were performed using a Brookhaven Instruments NanoBrook Omni phase analysis light scattering (PALS) instrument. This equipment was used to assess the surface charge of the various nanoparticle solutions dispersed in PGM. To prepare samples for this experiment, 1:100 dilutions were performed by method of serial dilution before running the experiments. Experiments were conducted at a 640 nm laser wavelength. Data were

collected from ten 30-cycle measurements, with 5 second pauses between measurements. Blank NPs and the blank mucin solution were again measured as controls. All error for data is shown as 95% confidence intervals

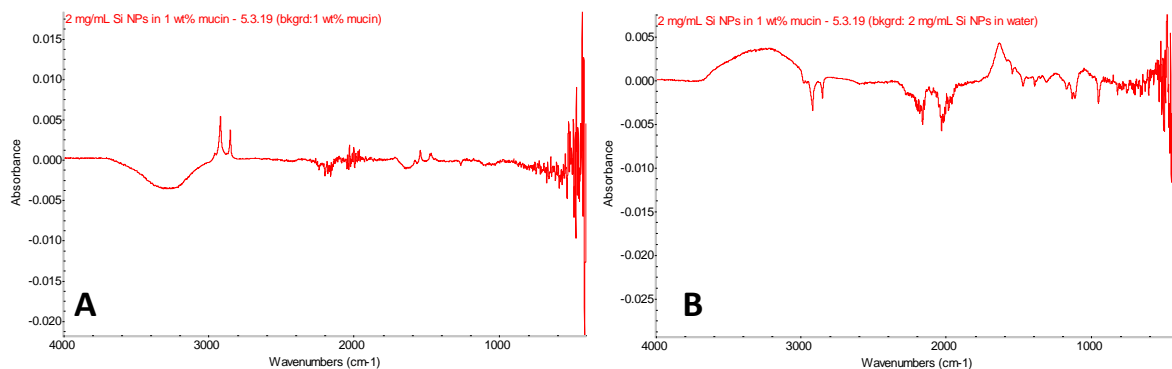
### 3.4. Results and Discussion

To confirm the presence of SiO<sub>2</sub> from the Stöber process, FTIR data was collected using an attenuated total reflectance (ATR) accessory on a Thermo Fisher Nicolet iS50 FTIR instrument. To sufficiently coat the ATR crystal, approximately 5 drops of a solution of 0.05 mg/mL silica NPs in isopropyl alcohol were dropped and dried on the crystal. Figure 18 shows the spectra of the pure silica NPs. The small C-H stretch peaks at 2900 cm<sup>-1</sup> are likely due to remnant TEOS that was not removed through the dialysis filtration step (small amounts of TEOS should be expected as dialysis is a concentration driven membrane separation). The peaks at 1090 cm<sup>-1</sup> and 800 cm<sup>-1</sup> correspond to Si-O-Si bonds, and the peak at 950 cm<sup>-1</sup> corresponds to Si-OH bonds in the silica NPs.



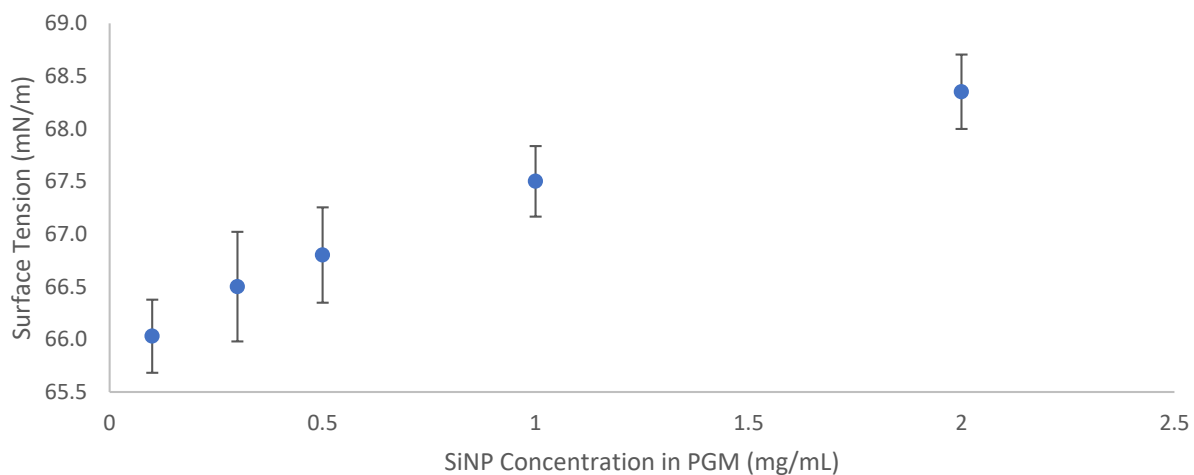
**Figure 18:** IR spectrum of dried silica nanoparticles (air background).

Figure 19 shows IR spectra of the 2 mg/mL NP PGM solution with respect to different backgrounds. FTIR spectra shows no clear evidence of bonding between SiNP and PGM.



**Figure 19:** IR spectra of 2 mg/mL silica nanoparticles in 1% w/w PGM solution, run with different background subtractions: (A) blank 1% w/w PGM solution background, (B) 2 mg/mL silica nanoparticles in water background.

The effect of SiNPs on the surface tension of PGM was studied using the pendant drop technique. The surface tensions of water, blank PGM at 10 mg/mL, blank SiNPs at 2 mg/mL, and PGM (10 mg/mL) + SiNP (10 mg/mL) were referenced and used as controls. Results for these can be seen in Table 3 and Figure 20 below. From these results, we gather that the surface tension of SiNP loaded PGM does not deviate much from the surface tension of blank PGM, however slight changes were observed in the data collected. Higher surface tension values were observed for solutions with higher concentrations of SiNPs in PGM solutions. It was interesting to see the surface tension of the highest concentration studied (2 mg/mL), was closest to the surface tension of blank PGM and that lower NP concentrations caused the surface tension to deviate. We can conclude that at the studied concentrations mucin dominates at the interface.



**Figure 20:** Surface tension values for PGM solutions increase with increasing SiNP concentration.

**Table 3:** Concentration of SiNPs in PGM solutions do not have significant effects on the surface tension as measured by pendant drop.

Sample Name	SiNP Conc. (mg/mL)	PGM Conc. (mg/mL)	SFT (mN/m)	±95% Confidence Interval
SiNP Control	2	0	77.13	0.1425
PGM Control	0	10	68.36	0.3036
Water	0	0	78.23	0.3036
0.1 mg/mL	0.1	10	66.03	0.3470
0.3 mg/mL	0.3	10	66.5	0.5206
0.5 mg/mL	0.5	10	66.8	0.4524
1 mg/mL	1	10	67.5	0.3346
2 mg/mL	2	10	68.35	0.3532
10 mg/mL	10	10	66.67	0.3532

The tabulated ZP data for the PGM solutions with SiNPs added, along with the controls, are shown in Table 4. The ZP of the SiNP control ( $-26.79 \pm 3.34$  mV) agrees with literature values.<sup>41</sup> The ZP of the blank NPs is 5-15 mV less in magnitude than literature values, which were measured in water with a pH of 7.4.<sup>41</sup> The blank NPs were dispersed in water with pH 5.4 which accounts for their lower ZP and thus lower stability. Higher absolute values of zeta potential mean that the colloidal system is more stable, thus allowing a suspension that can be used for adsorption mechanism in drug delivery systems.<sup>42, 43</sup>

The ZPs of the NP loaded PGM samples is seen to decrease in magnitude as NP concentration increase, however all values of NP loaded samples are higher than the ZP values of native PGM. The SiNP seem to cause the mucin molecules to interact more with itself thereby making it more stable when added in small concentrations. This suggests that even lower NP concentrations would be more adequate to stabilize SiNP loaded PGM samples for biomedical applications and this hypothesis should be tested.

**Table 4:** Zeta potential values for 10 mg/mL PGM solutions with added SiNP are electropositive and show additional stability versus the PGM control. Increased SiNP concentration moves the zeta potential towards the isoelectric point region.

Sample Name	SiNP Conc. (mg/mL)	PGM Conc. (mg/mL)	pH	Zeta Potential (mV)	±95% Confidence Interval
SiNP Control	2	0	<b>7.203</b>	<b>-26.79</b>	3.34
PGM Control	0	10	<b>4.699</b>	<b>12.14</b>	0.62
<b>0.1 mg/mL</b>	0.1	10	<b>3.699</b>	<b>18.63</b>	0.59
<b>0.3 mg/mL</b>	0.3	10	<b>3.728</b>	<b>18.36</b>	0.54
<b>0.5 mg/mL</b>	0.5	10	<b>3.802</b>	<b>16.18</b>	0.19
<b>1 mg/mL</b>	1	10	<b>3.683</b>	<b>14.11</b>	0.58
<b>2 mg/mL</b>	2	10	<b>3.684</b>	<b>13.22</b>	0.86

Zeta potential has been proven to be directly linked with particle size and aggregation of particles.<sup>16, 32-34</sup> From the zeta potential results of loaded SiNP PGM samples, the downward trend



suggests that the particles are approaching the isoelectric point (IEP) which would cause the particles to aggregate more and have larger diameters.<sup>16</sup> The IEP occurs when the net charge of the samples equal zero. At the IEP, the structure is more hydrophobic, more compact and less stable due to absence of inter-particle repulsive forces thus making it easier for particles to aggregate and precipitate.<sup>32-34</sup>

Knowing the relationship between zeta potential and particle size, the aggregation of silica nanoparticle loaded mucin samples were studied using dynamic light scattering to confirm this trend. The tabulated mean particle diameter in Table 5 shows that the mean diameter of the solutions increases with an increase in concentration of the SiNPs added to mucin. This is also due to mucin interacting more with itself when SiNPs were introduced in small concentrations. The SiNPs used in this experiment act similar to previously conducted studies relating ZP of proteins to the particle diameter.<sup>44</sup>

**Table 5:** Increase in SiNP concentration in 10 mg/mL PGM solution induces aggregation.

Sample Name	SiNP Conc. (mg/mL)	PGM Conc. (mg/mL)	Mean Diameter (nm)	±95% Confidence Interval (nm)
SiNP Control	2	0	<b>74.79</b>	21.80
PGM Control	0	10	<b>456.88</b>	151.7
<b>0.1 mg/mL</b>	0.1	10	<b>320.30</b>	126.40
<b>0.3 mg/mL</b>	0.3	10	<b>349.43</b>	138.33
<b>0.5 mg/mL</b>	0.5	10	<b>383.42</b>	144.12
<b>1 mg/mL</b>	1	10	<b>385.58</b>	133.02
<b>2 mg/mL</b>	2	10	<b>500.75</b>	155.73

Looking at ZP and DLS data together in Figure 21, we can see that as the zeta potential approaches the IEP (zero), the particles become more unstable and aggregation increases leading to larger particle diameters.

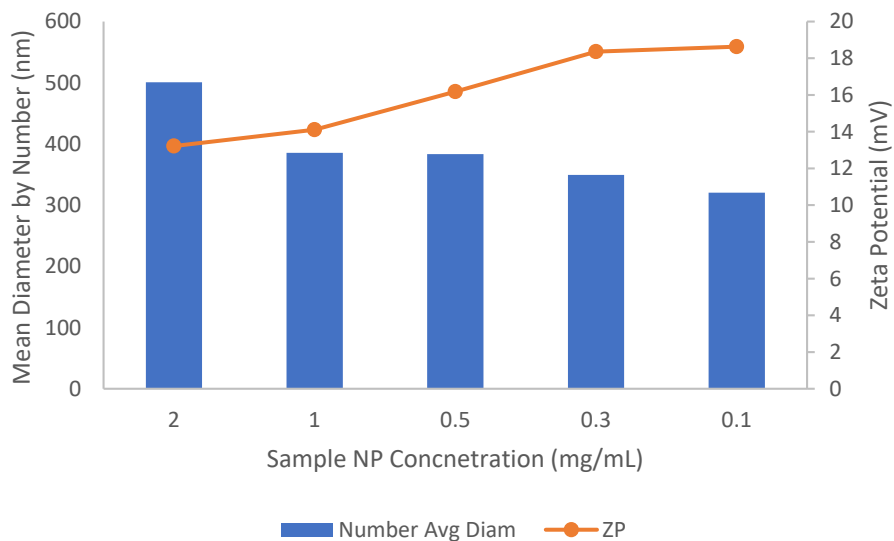


**Figure 21:** Lower zeta potential results in particles in solution aggregating more. Zeta potential approaches the isoelectric point region as SiNP concentration increases.

To study changes in the viscoelastic properties of the studied samples, frequency sweep experiments were carried out on the PGM + SiNP samples. The frequency sweeps were run at a strain located within the LVR of the sample and over a range of oscillation frequencies from 0.1-100 rad/s as seen in Figure 22 below.

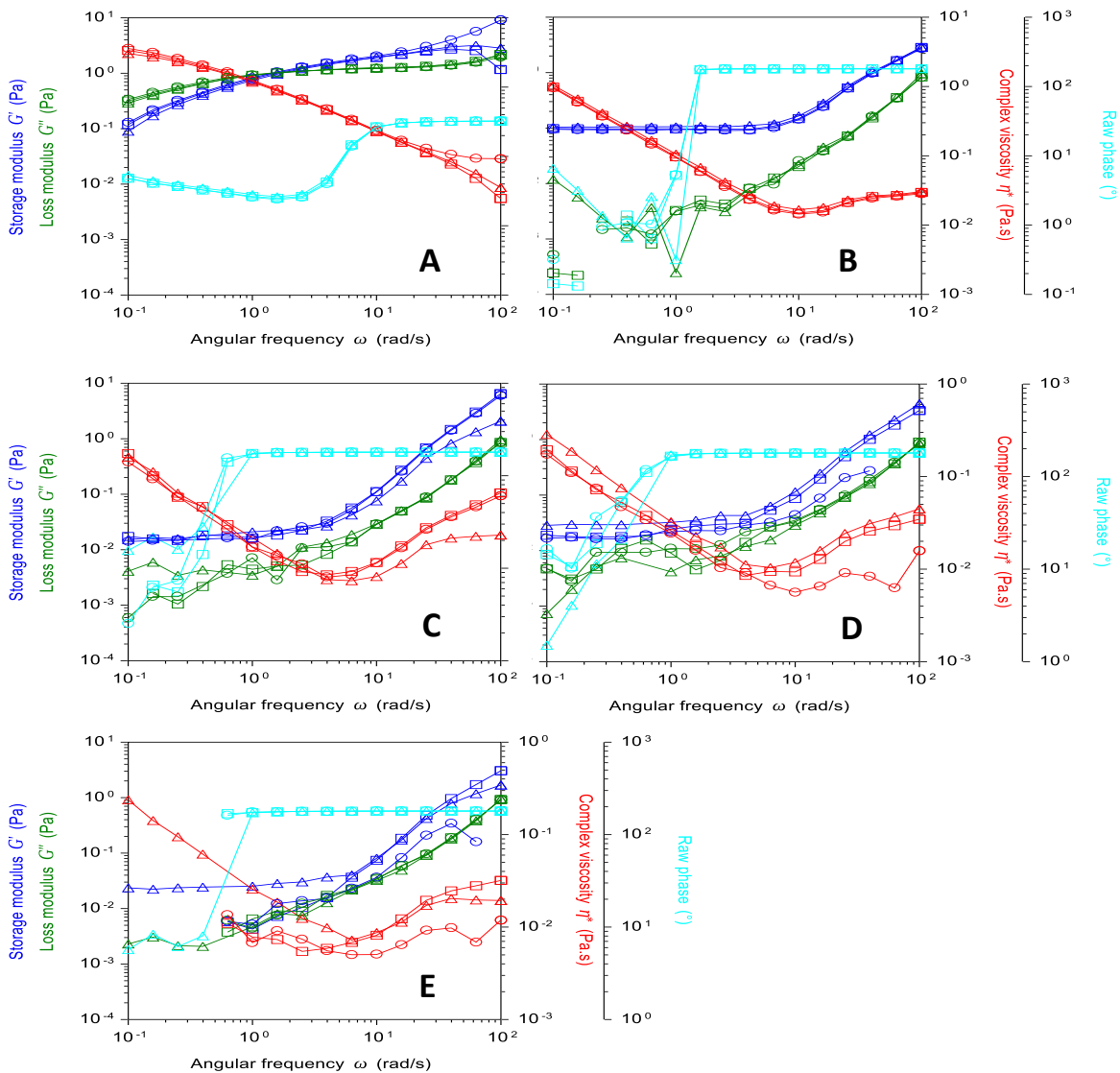


**Figure 22:** Rheology frequency sweeps on 1% w/w PGM samples with various SiNP concentration: (A) Blank PGM at 10 mg/mL with no nanoparticles, (B) 2 mg/mL MNPs + 10 mg/mL PGM, (C) 1 mg/mL MNPs + 10 mg/mL PGM, (D) 0.5 mg/mL MNPs + 10 mg/mL PGM, (E) 0.3 mg/mL MNPs + 10 mg/mL PGM.

Note that when the raw phase surpasses  $175^\circ$ , data become unreliable because the inertia of the rheometer dominates the measurement. All samples except the blank PGM run surpassed the  $175^\circ$  raw phase before a frequency of 1 rad/s, so the comparable data is limited to frequencies between 0.1-1 rad/s. Within this range of frequencies, storage moduli ( $G'$ ) dominated the loss

moduli ( $G''$ ) in all solutions with NPs, while the loss modulus dominated in the blank solution.  $G''$  of the NP solutions were consistently three orders of magnitude lower than  $G''$  of the blank solution. Additionally, the gap between  $G'$  and  $G''$  in the NP solutions trends towards larger separations at higher NP concentrations. The data suggests silica NPs increase the gel behavior ( $G'$  dominates  $G''$ ) of mucin in the low frequency range of 0.1-1 rad/s.

### 3.5. Conclusions

Unfunctionalized, uniform, monodisperse silica nanoparticles with mean diameter of 75 nm do not display significant evidence of chemical or physical interactions with mucins in 1 % w/w aqueous PGM solutions when added at concentrations of 2, 1, 0.5, 0.3, and 0.1 mg/mL. IR peaks indicating new chemical bonding were not found in the 2 mg/mL PGM solution, when subtracted from nanoparticle and mucin backgrounds. Zeta potential experiments show a decrease in charge as the concentration of the SiNPs in mucin increases. The trend observed suggests that the SiNPs present in mucin causing it to aggregate and approach the isoelectric point (charge of zero). Aggregation hypothesis was confirmed by running DLS particle sizing experiments. To improve stability of NPs in mucin solutions, even smaller NP concentrations (0-0.1 mg/mL) should be used to make the zeta potential far away from the isoelectric point and determine if a relative maximum zeta potential occurs within this range. Frequency sweeps should be rerun to increase the range of useable data.

The size of the Stöber process-synthesized NPs can be decreased by decreasing the amount of  $\text{NH}_4\text{OH}$ , which acts as a catalyst. There also exist studies that tabulate reaction recipes to achieve specific particle size<sup>45</sup> or model the predicted particle diameter as function of the relative volume of the reaction chemicals<sup>46</sup>. Future work can investigate the effects of larger or smaller NPs on mucin rheology by using such models to carefully control NP size. Eventually, we aim to functionalize silica nanoparticles with mucoadhesive nanoparticles and characterize their effects on mucin solution rheology.

## Chapter 4. Effect of Magnetic Nanoparticle Addition on Mucin Microstructure

### 4.1. Abstract

In this study we looked at the synthesis of iron oxide based nanoparticles using the Massart method. The interaction and binding of the synthesized MNPs to porcine gastric mucin (PGM) were studied using FT-IR, pendant drop, dynamic light scattering, zeta potential and rheology. FT-IR spectra collected suggest that no chemical interaction took place when making MNP loaded mucin samples. These nanoparticles however had an effect on the rheological properties of the mucin samples by increasing the gel behavior and as we observe the sol-gel transition occur at higher frequencies than that of neat PGM). An increase in the zeta potential of samples was seen to correlate to a decrease in the mean diameter measured using dynamic light scattering.

### 4.2. Introduction

Magnetic nanoparticles have gained a lot of attention in many fields due to their diverse and unique chemistry and their potential for many applications in a variety of fields. Their biocompatibility, injectability lack of toxicity, and ability to be manipulated using magnetic field makes it very attractive for research<sup>47</sup>. Magnetic nanoparticles have shown usefulness in the medical field for separation applications, contrast enhancing agents for MRI imaging, and drug delivery applications.<sup>48</sup>

The goal of this research is to determine the rheological, surface tension, and structural effects of the doping concentration of unfunctionalized magnetic NPs on aqueous mucin solutions. This research will establish a baseline to build future studies about the rheological effects of functionalized, mucoadhesive NPs in mucin solutions. Magnetic NP concentrations of 2, 1, 0.5, 0.3, and 0.1 mg/mL in 1% w/w mucin solutions were studied. Fourier transform infrared spectroscopy (FTIR), surface tension pendant drop, dynamic light scattering particle sizing (DLS), zeta potential Phase Analysis Light Scattering (PALS), and rheometer frequency sweeps were used to characterize the mucin solutions.

### 4.3. Materials and Methods

Iron (II) chloride tetrahydrate ( $(\text{Fe(II)Cl}_2 \cdot 4\text{H}_2\text{O})$ , 98%), iron (III) chloride hexahydrate ( $(\text{Fe(III)Cl}_3 \cdot 6\text{H}_2\text{O})$ , 98%), ammonium hydroxide ( $\text{NH}_4\text{OH}$ , 28-30%, ACS reagent) were purchased from Sigma-Aldrich and used as received. Hydrochloric acid ( $\text{HCl}$ , 37%, ACS reagent) was purchased from VWR and used as received.

*Iron Oxide Nanoparticle Synthesis.* Iron oxide magnetic nanoparticles (MNP) were synthesized via the Massart method <sup>49</sup>; wherein, ferric/ferrous salts are precipitated in aqueous alkaline media. In effort to reduce the oxidation of  $\text{Fe}^{2+}$  and  $\text{Fe}^{3+}$  ions, the reaction was performed under an inert atmosphere.  $\text{Fe}^{2+}$  and  $\text{Fe}^{3+}$  solutions were made by dissociating  $\text{Fe(II)Cl}_2 \cdot 4\text{H}_2\text{O}$  (3.18 g, 2 M) and  $\text{Fe(III)Cl}_3 \cdot 6\text{H}_2\text{O}$  (8.64 g, 3 M) in degassed  $\text{HCl}$  (2 M). In a reaction vessel equipped with condenser and mechanical stirrer,  $\text{NH}_4\text{OH}$  (38.5 mL, 0.7 M) was added to degassed Millipore Nanopure™ water and slowly heated to 60°C. The  $\text{Fe}^{2+}$  and  $\text{Fe}^{3+}$  solutions were injected simultaneously into the aqueous alkaline media under vigorous stirring conditions and allowed to react for 30 min at the elevated temperature. The reaction vessel was allowed to cool while maintaining constant agitation. Once the solution reached room temperature, the mixture underwent three washing cycles comprised of injecting degasified Nanopure™ water into the solution, allowing the solution to become well-mixed, separating the MNP by magnet, and decanting the supernatant. The MNP were then dried in a vacuum oven at 50 °C.

The morphology of the MNPs were examined using a Zeiss NEON Field-Emission scanning electron microscope (SEM) / Focused Ion Beam (FIB). Samples were prepared by sonicating in a pure volatile solvent and were drop-casted onto a UV-ozone treated Si wafer. Upon removal of the solvent, the particles were forced into closer proximity with each other, leading to further aggregation effects and artifacts in the sample (coffee ring effect). Images were taken using particles that were filtered through 0.2  $\mu\text{m}$  surfactant free cellulose acetate (SFCA) syringe filter and dried in a vacuum oven. SEM images are seen in Figure 23 below.

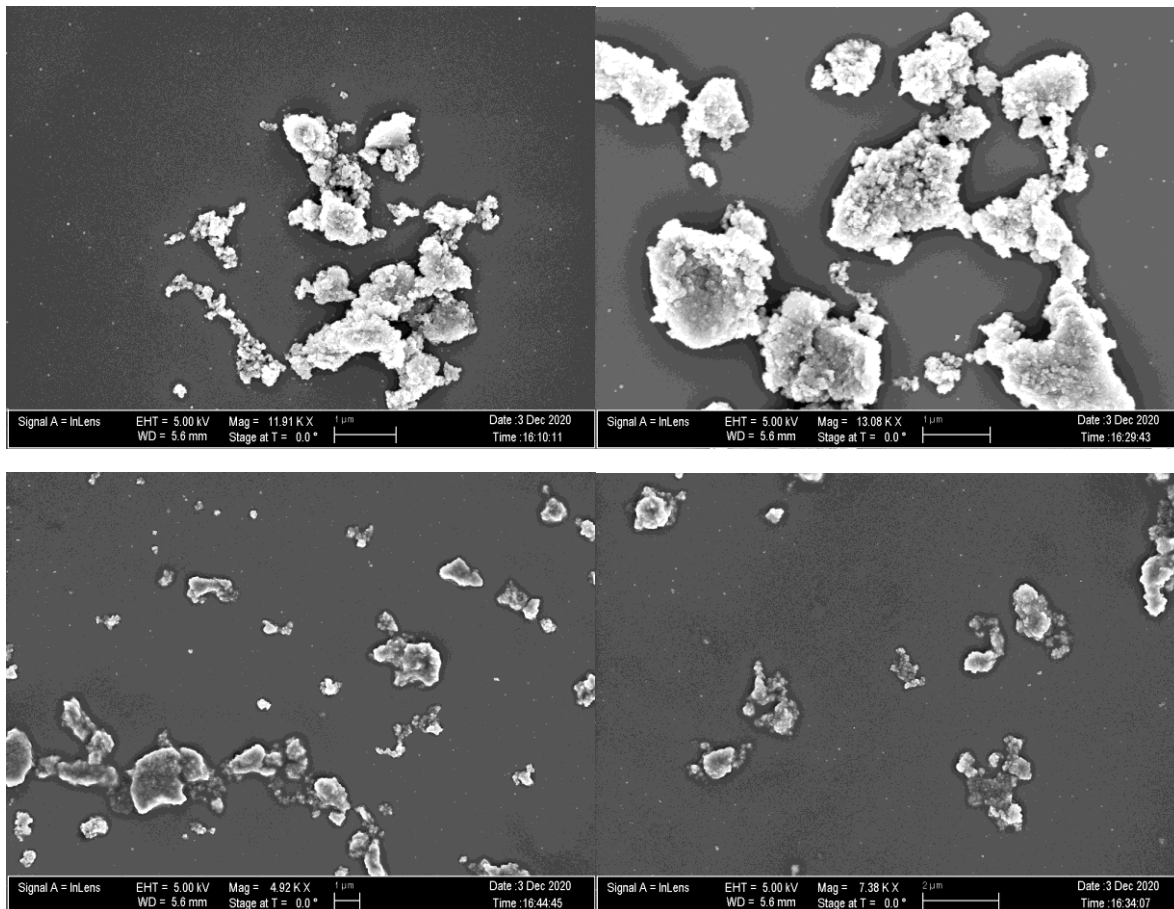


**Figure 23:** SEM micrographs of Massart method synthesized magnetic nanoparticles show irregular shape and agglomeration of MNPs. Imaging was done after nanoparticles were filtered with 0.2  $\mu\text{m}$  SFCA syringe filter.

It is observed that majority of the particles are fused together and smaller particles have agglomerated and aggregated together. The morphology is also very irregular, jagged, and more rigid as a result of using the Massart synthesis method. Bare MNPs tend to aggregate naturally without any surface modification when using this synthesis method. Iron oxide ( $\text{Fe}_3\text{O}_4$  and  $\text{Fe}_2\text{O}_3$ ) NPs also have a low solubility in water causing significant agglomeration and sedimentation. Upon redispersion, filtration, and drying, the MNPs underwent induced aggregation. Use of ultrasonication helped in redispersing the particles somewhat; however, this was not sufficient in keeping the particles stabilized.

Preparation of blank and magnetic nanoparticle-doped mucin solutions. Rehydrated mucin is used in this study as it is comparable structurally to native mucus and readily available. A blank mucin 10 mg/mL (1 wt%) solution was prepared with lyophilized Mucin from Porcine Stomach Type II from Sigma-Aldrich (PGM) and Nanopure™ water. The blank mucin solution was used as a control and reference for the MNP-doped mucin solutions.

After synthesis, the magnetic nanoparticles were very huge in size and so they were dispersed in Nanopure™ water and filtered using a 0.2 µm surfactant free cellulose acetate (SFCA) syringe filter. The filtrate was dried in a vacuum oven and particles were measured out to make NP solutions of 2, 1, 0.5, 0.3, and 0.1 mg/mL. PGM was added to each NP solution to make 1% w/w mucin solutions. To ensure thorough hydration of the mucins, all mucin solutions were sonicated for 30 minutes and refrigerated for 24 hours before experiments were run. All experiments were conducted at room temperature. The blank mucin solution was used as a control and reference for the magnetic NP-doped mucin solutions.

Pendant Drop. Surface tension measurements at room temperature were collected using a Krüss Drop Shape Analyzer-DSA25. This was used to measure the surface tension of PGM + MNPs. MNPs were made to 2, 1, 0.5, 0.3 and 0.1 mg/mL concentrations and 10 mg/mL of PGM was added to the solutions. After drops were dispensed, a wait time of 30 seconds was observed before collecting data. All error for data is shown as 95% confidence intervals.

Fourier Transforming Infrared Spectroscopy (FTIR). Physical characterization of mucin bound MNPs was confirmed using FTIR spectroscopy. Spectral data was acquired using a Thermo Fisher Nicolet iS50 instrument with a deuterated triglycine sulfate (DTGS) detector, attenuated total reflectance (ATR) accessory with diamond-ZnSe crystal and a XT-KBr beam splitter. Nanoparticles in isopropyl alcohol and NP: PGM solutions were drop-cast onto the ATR crystal for measurements at ambient temperature (approximately 23 °C).

Rheology. Rheological measurements were collected using a TA instruments Discovery Hybrid Rheometer II using Trios software (v5. on 00). A 40 mm cone with an angle of 2.013° was used to



perform frequency and flow sweeps the solutions containing MNP+ PGM solutions. The angled 40 mm geometry was chosen because the diameter was appropriate for samples with medium viscosity and the cone shape produces a smaller gap height closer to inside so the shear on the sample is constant.<sup>15</sup>

Before rheological measurements were taken for the samples, the linear viscoelastic regime (LVR) was determined for each concentration solution; this is an important step to determine the range in which the storage modulus ( $G'$ ) and the loss modulus ( $G''$ ) are independent of stress amplitude ( $\sigma_0$ ). This was done by performing a dynamic stress sweep to observe how the material responds to increasing deformation at a constant frequency and temperature. For the LVR experiment, a constant frequency of 1 rad/s was selected over a stress range of 0.01 to 100 Pa at 25 °C. The LVR was determined by choosing the average strain value that produces constant elastic moduli variable. Frequency sweep oscillation experiments were carried out on the 1, 2 and 5 wt% mucin solutions at each samples strain value related to the LVR results at 25 °C and 37 °C. over a 0.01 to 100 rad/s range.

Dynamic Light Scattering. DLS particle sizing was performed using a NanoBrook Omni PALS instrument equipped with Brookhaven Instruments Particle Solutions Software. This equipment was used to perform particle sizing of the PGM + MNP solutions. When running DLS particle sizing, sample must be transparent to allow the laser beams pass through to interact with the particles. To prepare samples, 1:100 dilutions were performed by method of serial dilution before running the experiments. Experiments were conducted using a 90-degree laser angle, and a 640nm laser wavelength. All error for data is shown as 95% confidence intervals.

Zeta Potential. Zeta potential experiments were performed using a Brookhaven Instruments NanoBrook Omni phase analysis light scattering (PALS) instrument. This equipment was used to assess the surface charge of the various nanoparticle solutions dispersed in PGM. To prepare samples for this experiment, 1:100 dilutions were performed by method of serial dilution before running the experiments. Experiments were conducted at a 640 nm laser wavelength. Data were collected from ten 30-cycle measurements, with 5 second pauses between measurements. Blank NPs and the blank mucin solution were again measured as controls. All error for data is shown as 95% confidence intervals

#### 4.4. Results and Discussion

To confirm the presence of Fe<sub>3</sub>O<sub>4</sub> from the Massart method, FTIR data was collected using an attenuated total reflectance (ATR) accessory on a Thermo Fisher Nicolet iS50 FTIR instrument. To sufficiently coat the ATR crystal, approximately 5 drops of a solution of 2 mg/mL magnetic NPs in ethanol were dropped and dried on the crystal. Figure 24 shows the spectra of the pure MNPs. The intense peaks observed at 556 cm<sup>-1</sup> and 435 cm<sup>-1</sup> are attributed to the stretching vibration mode associated to the metal-oxygen Fe-O bonds in the crystalline lattice of Fe<sub>3</sub>O<sub>4</sub> which confirms our synthesis was successful.

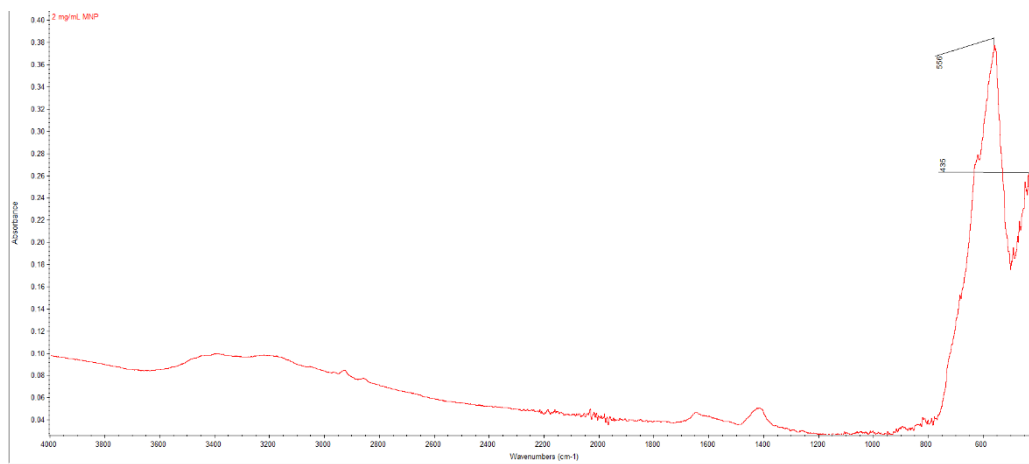


**Figure 24:** IR spectrum of dried magnetic nanoparticles (air background).

Figure 25 shows IR spectra of the 2 mg/mL MNP + 10 mg/mL PGM, 10 mg/mL PGM, and 2 mg/mL MNP solutions. All backgrounds taken were air and have been subtracted from spectra. The absence of new peaks in the 2 mg/mL MNP + 10 mg/mL MNP spectra indicates a lack of chemical bonding or formation of new products from the interaction between the NPs and the mucin.

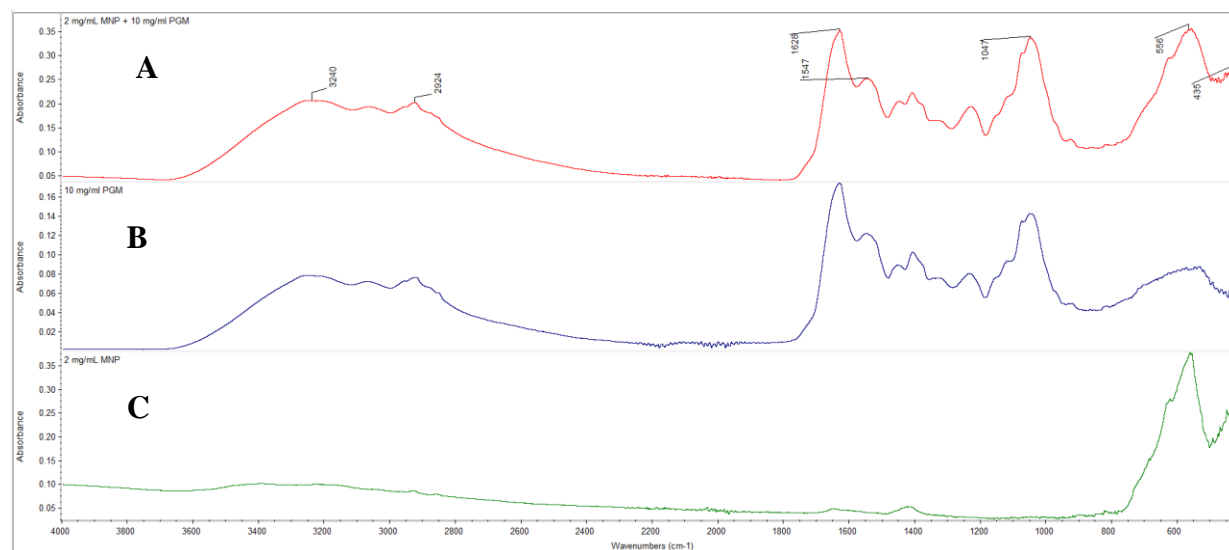


**Figure 25:** FT-IR stacked spectra showing absence of new functional groups in MNP loaded PGM samples (A): 2 mg/mL MNP + 10 mg/mL PGM; (B): 10 mg/mL PGM; (C): 2 mg/mL MNP

From the PGM spectra (B), a broad O-H stretch from the carboxylic acid groups (COOH) present is observed in the  $3240$  to  $3000\text{ cm}^{-1}$  range. C-H stretch is also seen in the  $\sim 2900$ - $2800\text{ cm}^{-1}$  range.<sup>11, 50</sup> Further down, the peaks found at wave numbers  $1628\text{ cm}^{-1}$  and  $1547\text{ cm}^{-1}$  correspond to Amide I (C=O) and II (C-N and N-H) groups respectively.<sup>11, 51</sup> Strong peaks at  $1047\text{ cm}^{-1}$  represents sulfoxide (S=O) stretching. Disulfide bonding has also been known to play a role in the network formation of mucin<sup>52-54</sup>. These are seen at strong peaks observed at  $556\text{ cm}^{-1}$ .

Most biochemical reactions occur on the surface of various tissues and organs that are lined with mucin instead of in solution, therefore, it is very important to know the surface characteristics of nanoparticles in mucin for biological applications and studies.<sup>55</sup> The surface tension of MNP loaded PGM samples and controls were collected and shown in Table 6 below. The surface tension values of the nanoparticle loaded mucin solutions did not deviate much from the surface tension of the control (10 mg/mL PGM solution without MNP). We can conclude that at the studied concentrations of nanoparticle solutions, mucin properties dominate at the surface of the solutions.

**Table 6:** PGM properties dominate at the surface level. Loading PGM samples with MNPs of different concentrations has very little effect on the surface tension values.

Sample Name	MNP Conc. (mg/mL)	PGM Conc. (mg/mL)	SFT (mN/m)	±95% Confidence Interval (nm)
MNP Control	2	0	76.21	0.421
PGM Control	0	10	68.36	0.304
Water	0	0	78.23	0.304
0.1 mg/mL	0.1	10	67.42	0.254
0.3 mg/mL	0.3	10	68.67	0.180
0.5 mg/mL	0.5	10	67.48	0.186
1 mg/mL	1	10	67.21	0.267
2 mg/mL	2	10	65.43	0.254
10 mg/mL	10	10	65.41	0.620

Zeta potential experiments were conducted to investigate the changes in the charge of PGM upon adding MNPs. The zeta potential property is highly dependent on the pH of the sample and so the pH values of the solutions were measured before running experiments. From Table 7 below, we see that the pH of the MNP loaded PGM samples do not change significantly and so the zeta potential of the MNP samples did not vary too much.

**Table 7:** Zeta potential depends the pH of the solution. Very little variation in the pH of the different samples causes ZP values by much.

Sample Name	MNP Conc. (mg/mL)	PGM Conc. (mg/mL)	pH	Zeta Potential (mV)	±95% Confidence Interval (nm)
MNP Control	2	0	5.944	-1.01	1.760
PGM Control	0	10	4.699	-0.36	1.376

<b>0.1 mg/mL</b>	0.1	10	4.973	0.76	1.965
<b>0.3 mg/mL</b>	0.3	10	4.947	1.19	1.463
<b>0.5 mg/mL</b>	0.5	10	4.867	-0.92	1.624
<b>1 mg/mL</b>	1	10	4.365	2.29	0.880
<b>2 mg/mL</b>	2	10	4.909	2.48	0.953

The zeta potential values stayed around the isoelectric point and cross twice indicating that the samples were aggregating a lot. This was investigated by performing particle sizing experiments using dynamic light scattering. Particle sizing results shown in Table 8 below recorded a fluctuation in the size of the particles in relation to the concentration of nanoparticles present in the mucin solutions. Overall, it was observed that the MNPs caused the mucin to swell in solution, but this was not directly related to the concentration of the MNPs in solutions.

**Table 8:** Failure of large magnetic nanoparticles to bind to mucin structure caused variation in particle mean diameter of MNP +PGM solutions.

<b>Sample Name</b>	<b>MNP Conc. (mg/mL)</b>	<b>PGM Conc. (mg/mL)</b>	<b>Mean Diameter (nm)</b>	<b>±95% Confidence Interval (nm)</b>
<b>MNP Control</b>	2	0	276.03	97.96
<b>PGM Control</b>	0	10	240.69	67.24
<b>0.1 mg/mL</b>	0.1	10	345.04	115.3
<b>0.3 mg/mL</b>	0.3	10	273.77	120.7

<b>0.5 mg/mL</b>	0.5	10	391.18	138.2
<b>1 mg/mL</b>	1	10	244.95	107.2
<b>2 mg/mL</b>	2	10	228.34	81.20

Studies<sup>56</sup> have shown that the binding and transporting capabilities of mucin are highly dependent on the size and zeta potential of the loaded nanoparticles. The cross linked mucin fibers present in mucus allow for easy binding of particles, however particles of large diameter such as the MNPs with a mean diameter of 228.34 nm will have less surface area which can affect the interaction and binding of particles to the mucin fibers.<sup>56</sup>

It was expected that 2 mg/mL would have the highest mean diameter by number, however the data does not follow our assumptions and this is likely due to the MNPs falling out of solution because they are too large and unable to bind to the mucin which would explain the variation in the mean diameter data.

To further study the relationship between size and charge in NMP loaded PGM solutions zeta potential and particle diameter were graphed below in Figure 26 and it was observed that the charge increased whenever the diameter of the particle became smaller. For biomedical applications, the ideal zeta potential would be far away from the isoelectric point and particle diameter be smaller than what was observed in my results so as to avoid aggregation of particles that could lead to transport issues and complications.

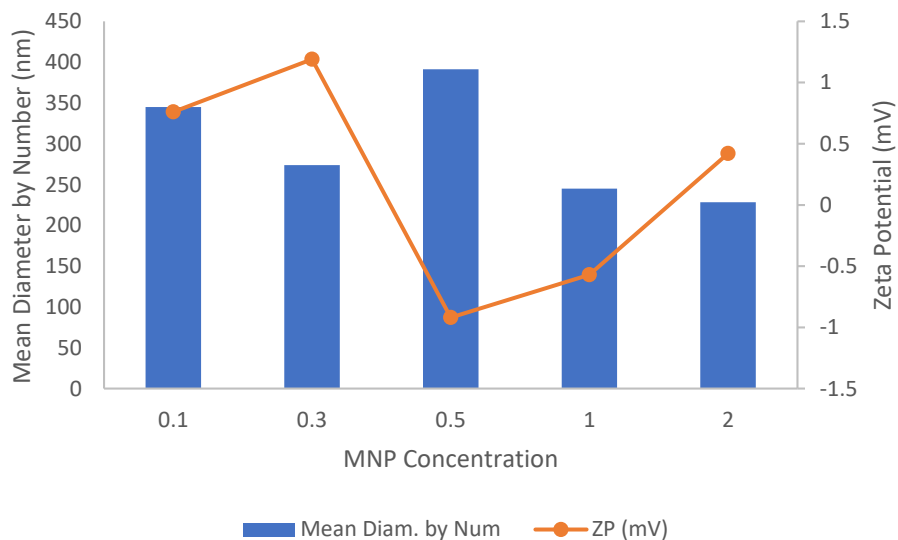


**Figure 26:** DLS and ZP results for nanoparticle loaded PGM show a positive increase in charge with decreasing mean diameter.

Changes in the viscoelastic properties of the MNP samples were studied by performing frequency sweep experiments at each samples determined LVR. The LVR information gives frequency sweep operating range where the storage modulus ( $G'$ ) and the loss modulus ( $G''$ ) are independent of stress amplitude ( $\sigma_0$ ). Frequency sweeps were done over a range of 0.1 to 100 rad/s as seen in Figure 27 below.

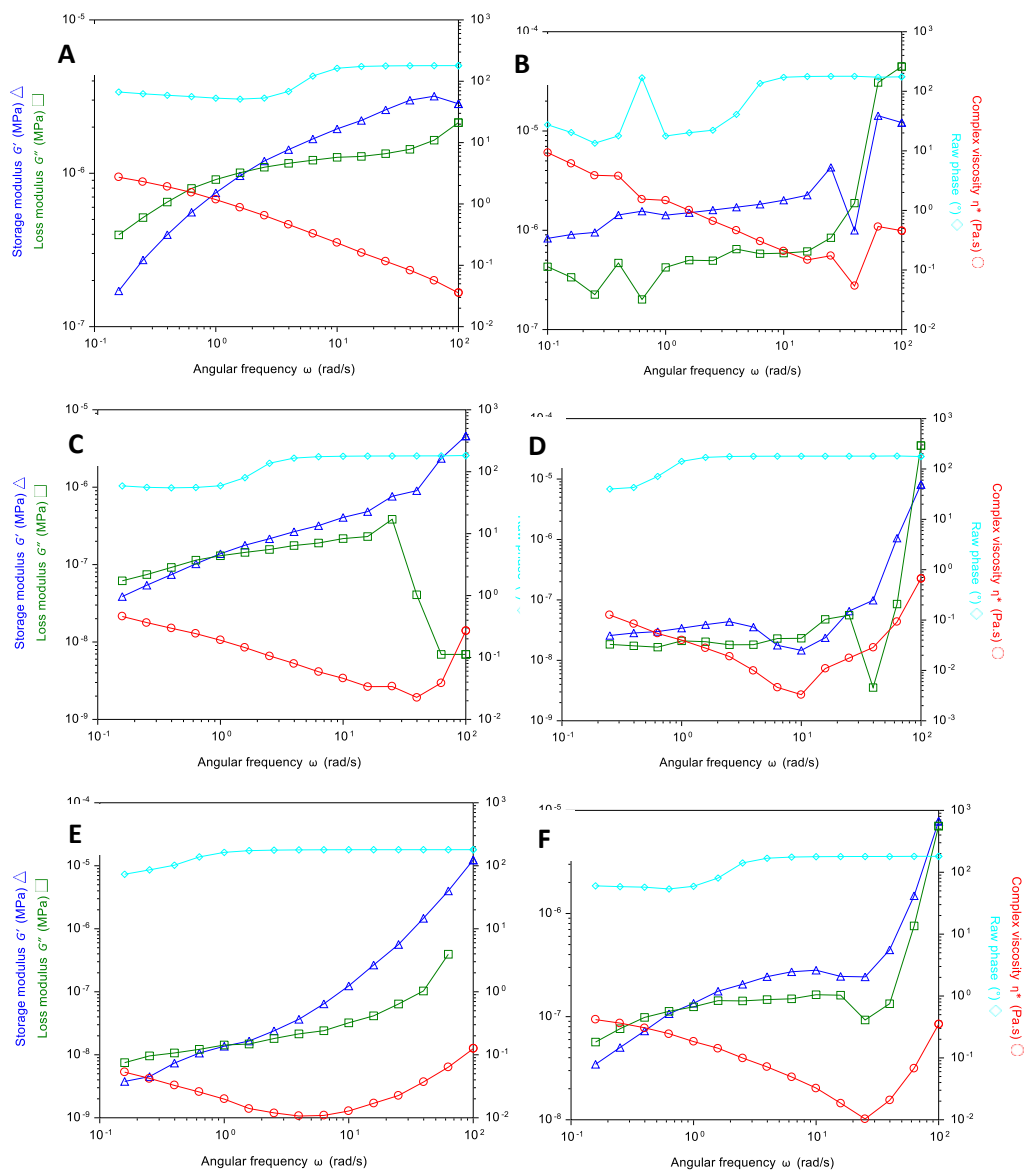


**Figure 27:** Frequency sweeps on 1% w/w PGM samples with various MNP concentrations: (A) Blank PGM at 10 mg/mL with no nanoparticles, (B) 2 mg/mL MNPs + 10 mg/mL PGM, (C) 1 mg/mL MNPs + 10 mg/mL PGM, (D) 0.5 mg/mL MNPs + 10 mg/mL PGM, (E) 0.3 mg/mL MNPs + 10 mg/mL PGM, (F) 0.1 mg/mL MNPs + 10 mg/mL PGM.

Within the frequency range studied, we observe that the presence of MNPs in the mucin samples causes the sol-gel transition to occur in the studied samples. When  $G'$  crosses over  $G''$  a gel-like response is observed. The concentrations and frequencies at which the transitions occur can be attributed to the change in ionic strength of the PGM solution after the addition of MNPs.<sup>2</sup>



<sup>24</sup> The raw phase is represented by the cyan data points in Figure 27. Above a raw phase of 175°, data becomes unreliable and inertia of the rheometer dominates the measurement. The raw phase surpassed 175°, in the 0.5 mg/mL and frequency sweep run and as a result of that the sol-gel transition occurs twice during the frequency sweep experiment.

#### *4.5. Conclusions*

The unfunctionalized magnetic nanoparticles do not display any evidence of chemical interactions with porcine gastric mucin in 1 % w/w aqueous PGM solutions when added at concentrations of 2, 1, 0.5, 0.3, and 0.1 mg/mL. IR peaks indicating new chemical bonding were not found in the 2 mg/mL PGM solution, when subtracted from nanoparticle and mucin backgrounds. Zeta potential did not vary significantly between the different concentrations, however the ZP values were proven to be directly related to the particle diameter and increased whenever the mean diameter by number decreased. Frequency sweeps performed showed an increase in gelation of PGM samples when loaded with MNPs.

For future work, MNPs at smaller diameters and lower concentrations should be used to avoid aggregation and nanoparticles falling out of solution. Suggested diameters would be 50-100nm range and concentrations would be below 0.1 mg/mL. The magnetic nanoparticles studied were also bare and unfunctionalized which affected the binding of the MNPs to the surface of the mucin. To improve the binding, the surface characteristic should be modified with different functional groups, surface charges, or by coating it with relevant substances.

## Chapter 5. Conclusions and Future Work

### 5.1. Study Conclusions

The results and findings in this work set the groundwork biomedical applications for understanding the influence of pH, temperature, concentration, and nanoparticle addition to porcine gastric mucin. Experiments conducted on PGM at 1, 2 and 5 wt% were seen to have noticeable impacts on the surface tension, rheological, and DLS properties. A uniformed decrease in the surface tension as the concentration of the PGM solutions increased was observed. This was due to the stronger intermolecular forces in the more dilute solutions that contained more water and therefore more hydrogen bonding. Rheology data showed that higher angular frequencies were required to achieve a sol-gel transition of PGM at higher concentrations.

Temperature increases showed changes in the sol-gel transition frequencies of PGM. The sol-gel transition to occurred at significantly higher frequencies when runs were performed at 37°C versus those at 25°C. This was due to a disruption of bonds and increased vibration of the molecules that required higher frequencies to stabilize the molecules. Varying the pH of PGM from 1 to 6 confirmed that PGM becomes a gel and a highly networked structure is observed under highly acidic conditions. Surface tension was seen to increase as the pH was decreased which was likely due to increased gelation and changes in the network structure as the sample became more acidic. ZP and DLS showed that at the isoelectric point (pH 3), the sample had the largest mean diameter by number compared to samples at different pH values.

FTIR data confirmed that the addition of both silica and magnetic nanoparticles had no chemical effect on PGM. DLS and ZP data were dependent on one another showing an increase in particle diameter as the zeta potential approached the isoelectric point at the concentrations studied. SiNP rheology data showed no sol-gel transition unlike the blank PGM samples. This indicates that a gel-like material response is maintained when SiNPs are incorporated into PGM samples.

The filtration and drying process of the magnetic nanoparticles caused the particles to aggregate in solution resulting in very large particle diameters that were unable to bind to the mucin structure.

## *5.2. Future Work Recommendations*

Future efforts for the work presented in Chapter 2 should explore the effect of gastric mucin while simultaneously varying pH at elevated temperatures. This is important especially for gastric mucin to model the true conditions in the stomach which is highly acidic and at 37 °C.

For the MNP mucin interaction discussed in chapter 4, I would recommend repeating the experiments performed but with smaller particles and at lower concentrations as an aim to stabilize samples and reduce aggregation of particles in solution. Getting the zeta potential values further away from the isoelectric point will reduce aggregation and improve transport of molecules for biomedical applications. Modification of both silica and magnetic nanoparticles with different functional groups, surface charges, or by coating it with relevant substances.

Future efforts on examining structure-property relationships for mucin solutions should explore the effect of gastric mucin while varying pH at elevated temperatures. The combined effects from varying both parameters are important for mucins in order to model the true conditions for transport across mucosal membranes where pH and temperature can vary significantly.

For the MNP mucin interaction study, repeating the experiments performed but with smaller particles and at lower concentrations is recommended. Using smaller particles will help stabilize MNP samples and reduce aggregation of particles in solution. Increase in stability corresponds to zeta potential values further from the isoelectric point which reduces aggregation and improves transport of molecules for biomedical applications.

Another recommendation would be to modify both silica and magnetic nanoparticles with different functional groups and/or net surface charges—either natively or by surface modification with relevant substances. Zeta potential and dynamic light scattering experiments for native mucin at 10 mg/mL and should be repeated to improve consistency of values.

## Appendices

### Appendix A: Sample Preparation Methods

*A1. Mucin Solutions:* Mucin samples were prepared by rehydrating powdered porcine gastric mucin (PGM) Type II in Nanopure™ water that is produced in house using a Millipore Synergy® Water Purification System #SYNS0HFUS with an EMD Millipore CDUFBI001 Biopak Ultrafiltration Cartridge. PGM was obtained from Sigma Aldrich (CAS 84082-64-4) and the powder was refrigerated when not in use. Samples were prepared at 10 mg/mL, 20 mg/mL, and 50 mg/mL. After rehydration, samples were sonicated for 30 minutes to mix and refrigerated for 24 hours. Samples were also sonicated for 30 minutes before running tests for surface tension, DLS, ZP and rheology. To prepare mucin solutions for DLS and zeta potential measurements, previously prepared mucin solutions were serially diluted twice using Nanopure™ water to 0.1, 0.2, and 0.5 mg/mL to make characterization possible.

*A2. Mucin pH solutions:* When preparing discrete PGM samples for pH studies, the pH of serial diluted (x100) PGM samples was changed using 0.01 M nitric acid (HNO<sub>3</sub>) and 0.01 M sodium hydroxide (NaOH) buffers by adding drops and measuring. The pH meter used when preparing the samples is a Thermo Scientific™ Orion™ Dual Star™ pH and ISE Benchtop Meter.

## Appendix B: Operating Procedures

### B1. Surface Tension

Surface tension measurements were taken using the pendant drop technique on a Krüss Drop Shape Analyzer-DSA25. Before experiments, the instrument was calibrated by adjusting the camera focus, specifying the needle diameter, selecting the region of interest, and setting the measuring lines. A 0.51mm diameter needle was used for pendant drop experiments. It was important to make sure the needle is straight and not tilted, the camera is in focus the drop is not deformed and that the magnification is not too high or too low. The baseline is used to determine the part of the drop that will be used for analysis, to select the area for measurement. It should be placed at the top of the drop and if applied correctly, the fit line generated from the software will correspond exactly to the profile of the whole drop<sup>57</sup> as shown in Figure 28 below.

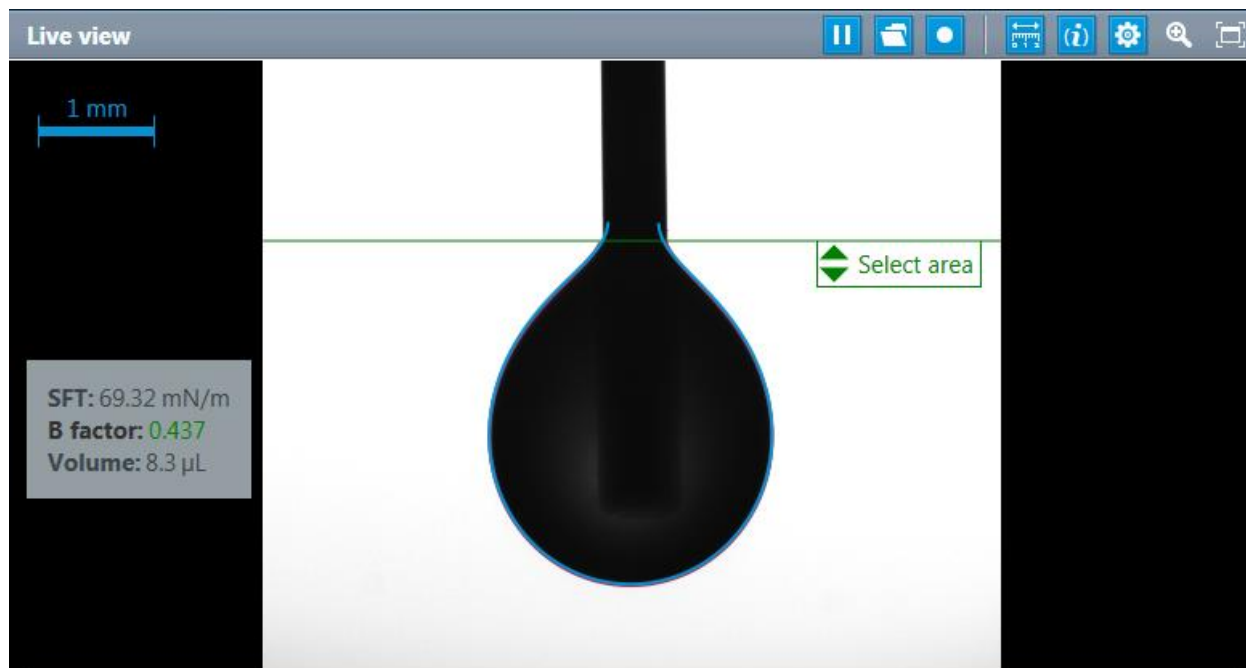


**Figure 28:** Representative image of static pendant drop.

## *B2. Rheology*

Rheology experiments were collected using a TA instruments Discovery Hybrid Rheometer II using Trios software (v5.00). A 40 mm cone with an angle of  $2.013^\circ$  was used to perform frequency and flow sweeps on the solutions containing PGM at various concentrations. A 40 mm cone geometry was chosen because the diameter was appropriate for samples with medium viscosity and the cone shape produces a smaller gap height closer to inside so the shear on the sample is constant <sup>15</sup>.

Stress sweep experiments were carried out at a constant frequency of 1 rad/s was selected over a stress range of 0.01 to 100 Pa at 25 and 37°C to determine the LVR. The LVR was determined by choosing the average strain value that produces constant elastic moduli variable. Experiment setup for determining LVR is shown in Figure 29 below.

Geometry: 40mm 2.013° cone plate, Peltier plate Steel - 111931      Procedure: AC Flow Sweep

Diameter: 40.0 mm  
 Cone angle: 02:00:45 deg:min:sec  
 Truncation gap: 53.0 μm  
 Trim gap offset: 50.0 μm  
 Loading gap: 45000.0 μm  
 Material: Stainless steel  
 Environmental system: Peltier plate  
 Serial number: 111931  
 Minimum sample volume is 0.588763 mL

⊖ Constants  
 ⊖ Notes

1: Flow Sweep

Environmental Control  
 Temperature: 25 °C  Inherit Set Point  
 Soak Time: 0.0 s  Wait For Temperature

Test Parameters  
 Logarithmic sweep  
 Shear rate: 1.0e-3 1/s to 1.0 1/s  
 Points per decade: 5

Steady state sensing  
 Max. equilibration time: 45.0 s  
 Sample period: 30.0 s  
 % tolerance: 10.0  
 Consecutive within: 3  
 Scaled time average

Procedure: Initial Strain Sweep OI

1: Flow Sweep

Environmental Control  
 Temperature: 25 °C  Inherit Set Point  
 Soak Time: 0.0 s  Wait For Temperature

Test Parameters  
 Logarithmic sweep  
 Shear rate: 1.0e-3 1/s to 1.0 1/s  
 Points per decade: 5


Steady state sensing  
 Max. equilibration time: 45.0 s  
 Sample period: 30.0 s  
 % tolerance: 10.0  
 Consecutive within: 3  
 Scaled time average

⊖ Controlled Rate Advanced  
 ⊖ Data acquisition  
 ⊖ Step termination

**Figure 29:** Rheology stress sweep experiments to determine LVR .

### B3. Dynamic Light Scattering

Dynamic light scattering data was collected using NanoBrook Omni PALS instrument equipped with Brookhaven Instruments Particle Solutions Software. Experiments were conducted using a 90-degree laser angle, and a 640nm laser wavelength. Samples were serial diluted twice (x100) before running experiments. Experiment setup is shown below in Figure 30.



Forward Scattering   
  90 Degree   
  Backscattering    [i](#)


Correlator Layout

General    [i](#)

Wavelength  nm    [i](#)

Cell Type     [i](#)

- Identification
- Instrument Parameters
- Measurement
  - Parameters
  - Automation
  - Time Dependent
- Sample Parameters
  - Liquid
  - Particle
- Data Analysis
  - Normalization
  - Size Distribution
  - MW Analysis



Temperature  deg C    [i](#)  
 Set Duration  seconds    [i](#)  
 Equilibration Time  seconds    [i](#)


Dust Rejection

Particle Size

< 10 nm    [i](#)  
 10 nm to 50 nm  
 50 nm to 250 nm  
 250 nm to 500 nm  
 > 500 nm


Apply Dust Filter    [i](#)

- Identification
- Instrument Parameters
- Measurement
  - Parameters
  - Automation
  - Time Dependent
- Sample Parameters
  - Liquid
  - Particle
- Data Analysis
  - Normalization
  - Size Distribution
  - MW Analysis



Total Measurements     [i](#)  
 Time Interval Between Measurements  seconds    [i](#)

- Identification
- Instrument Parameters
- Measurement
  - Parameters
  - Automation
  - Time Dependent
- Sample Parameters
  - Liquid
  - Particle
- Data Analysis
  - Normalization
  - Size Distribution
  - MW Analysis



Refractive Index of Particles

Real     [i](#)  
 Imaginary     [i](#)

Uniform Spheres    [i](#)   
  Thin Shells    [i](#)

Concentration  mg/mL    [i](#)

- Identification
- Instrument Parameters
- Measurement
  - Parameters
  - Automation
  - Time Dependent
- Sample Parameters
  - Liquid
  - Particle
- Data Analysis
  - Normalization
  - Size Distribution
  - MW Analysis

**Figure 30:** Dynamic light scattering experiment setup.



#### B4. Zeta Potential

Zeta potential experiments were performed using a Brookhaven Instruments NanoBrook Omni phase analysis light scattering (PALS) instrument. This equipment was used to assess the surface charge of the various nanoparticle solutions dispersed in PGM. To prepare samples for this experiment, 1:100 dilutions were performed by method of serial dilution before running the experiments. Experiments were conducted at a 640 nm laser wavelength. Data were collected from ten 30-cycle measurements, with 5 second pauses between measurements. Experimental setup for zeta potential is shown below in Figure 31.

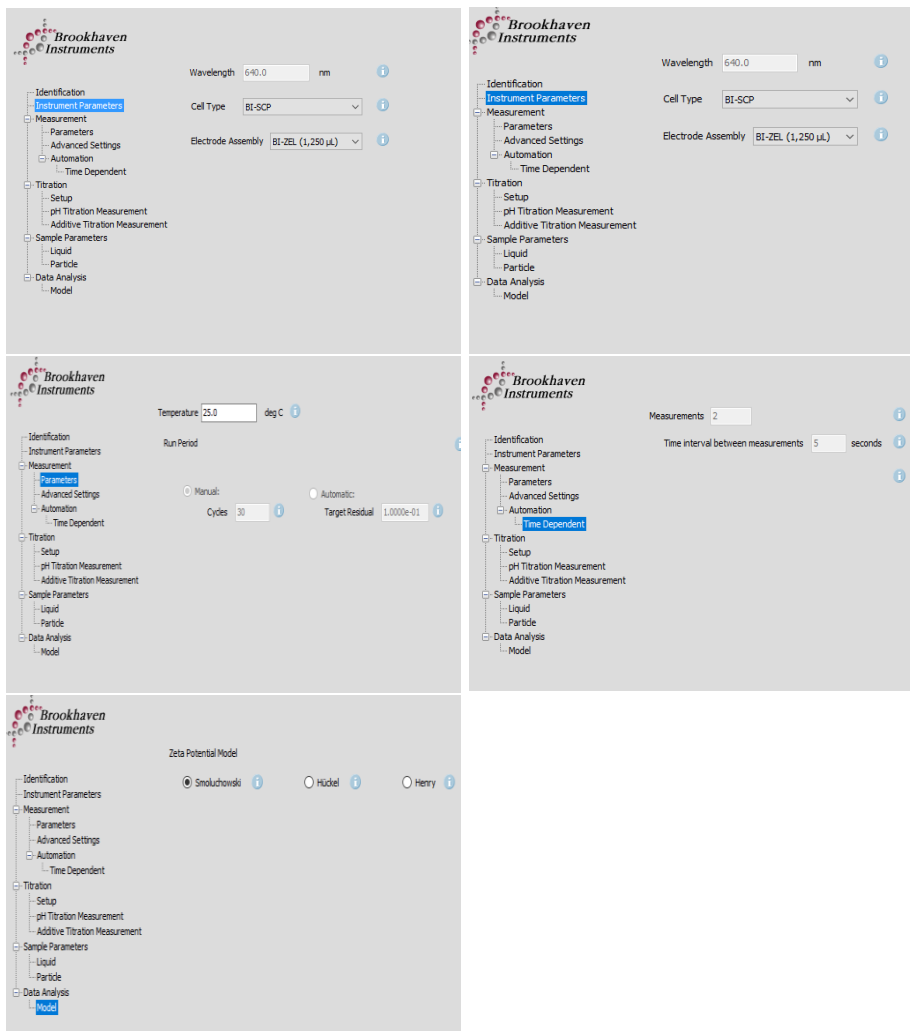


Figure 31: Zeta potential experimental setup.

### *B5. Fourier Transform Infrared Spectroscopy (FTIR)*

FT-IR data was acquired using a Thermo Fisher Nicolet iS50 instrument with a deuterated triglycine sulfate (DTGS) detector, attenuated total reflectance (ATR) accessory with diamond-ZnSe crystal and a XT-KBr beam splitter. SiNPs were dispersed in isopropyl alcohol and MNPs were dispersed in ethanol. NP: PGM solutions were drop-cast onto the ATR crystal for measurements at ambient temperature (approximately 23 °C).

## Appendix C: Supplementary Data

Figures 32 - 34 show static surface tension (SFT) data of different solvents discussed in Chapter 2. These data were obtained using the pendant drop method.

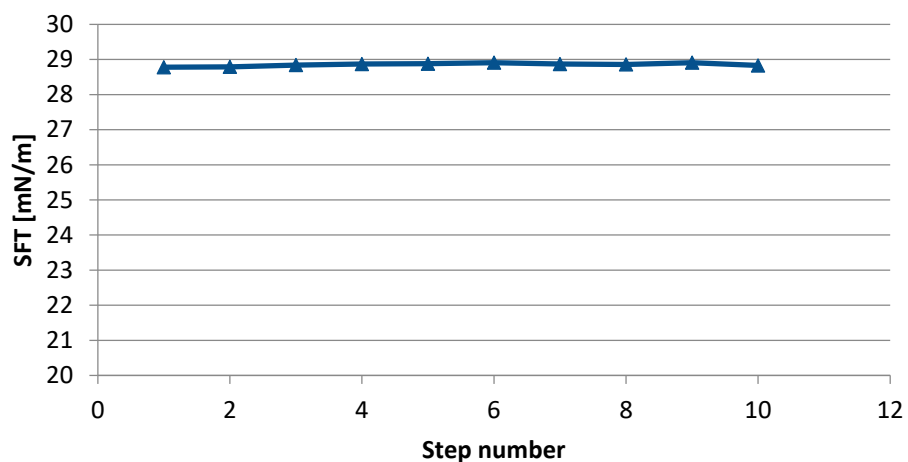


**Figure 32:** Surface tension of hexadecane at 37 °C.

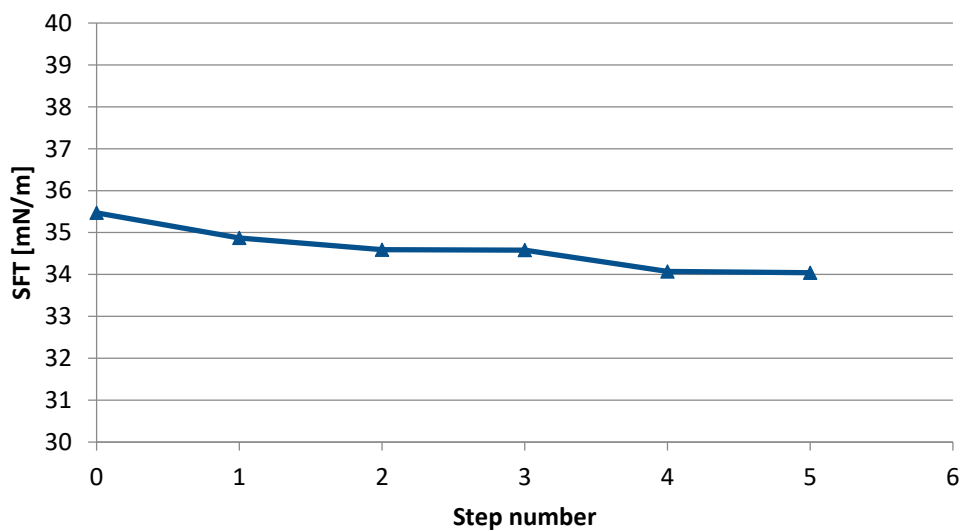


**Figure 33:** Surface tension of pyridine at 25 °C.

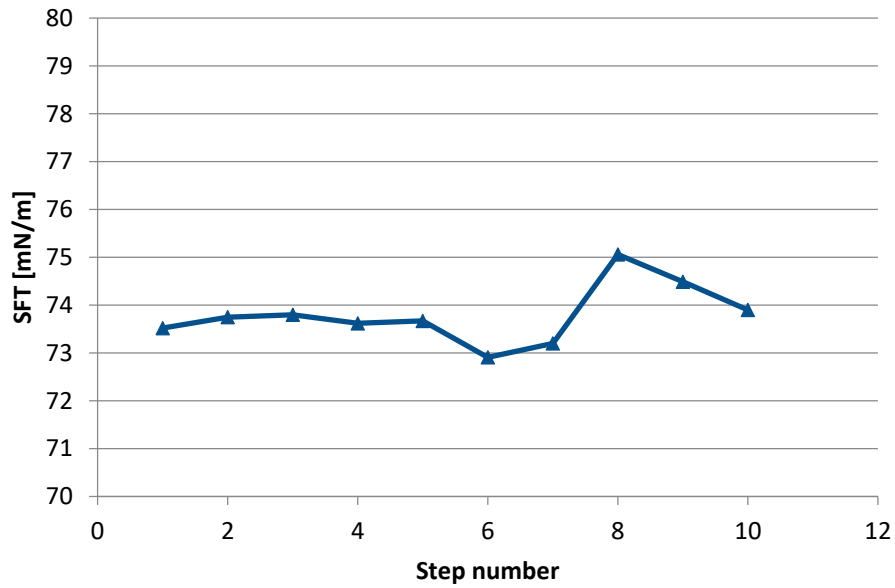


**Figure 34:** Surface tension of Nanopure™ water at 25 °C.

Figures 35 - 40 show rheology data for determining the LVR for PGM at 1, 2, and 5 wt% at 25 °C and 37 °C.

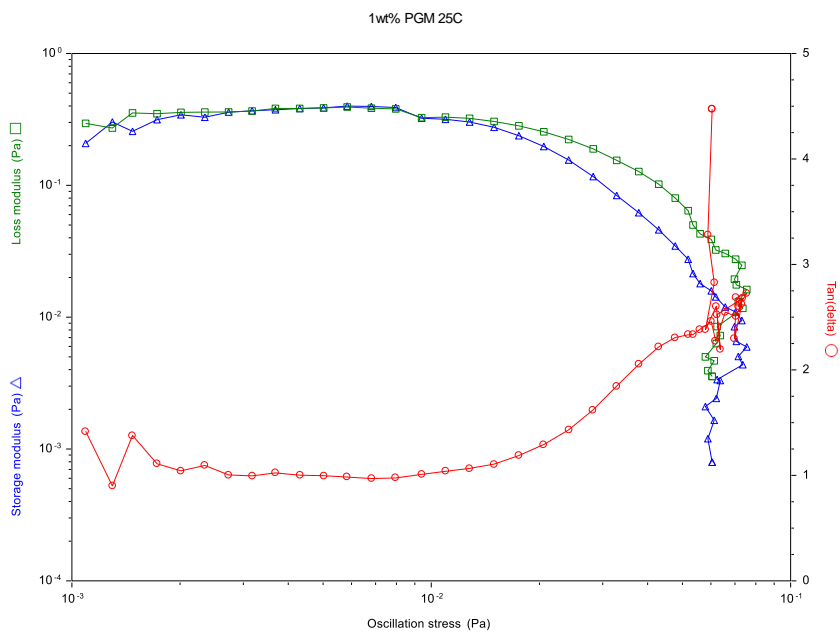


**Figure 35:** Dynamic stress sweep of 1 wt% PGM at 25 °C.

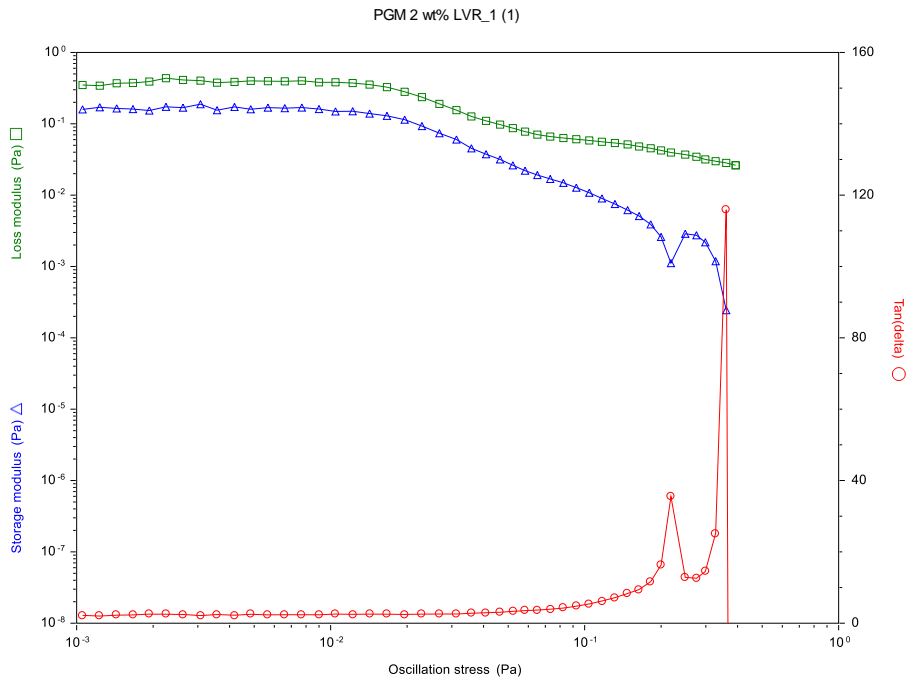


**Figure 36:** Dynamic stress sweep of 2 wt% PGM at 25 °C.

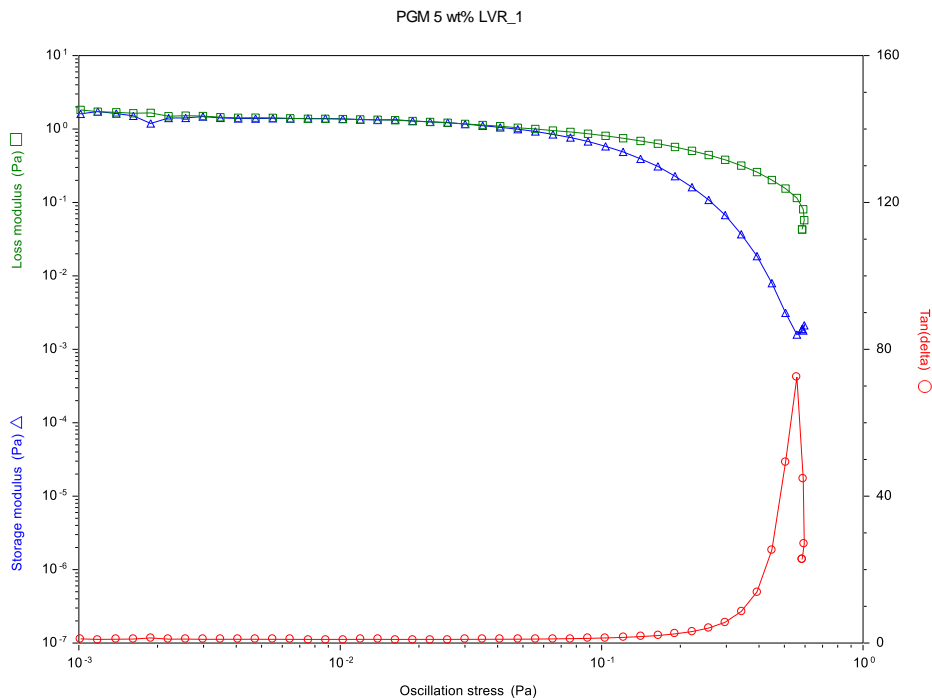


**Figure 37:** Dynamic stress sweep of 5 wt% PGM at 25 °C.

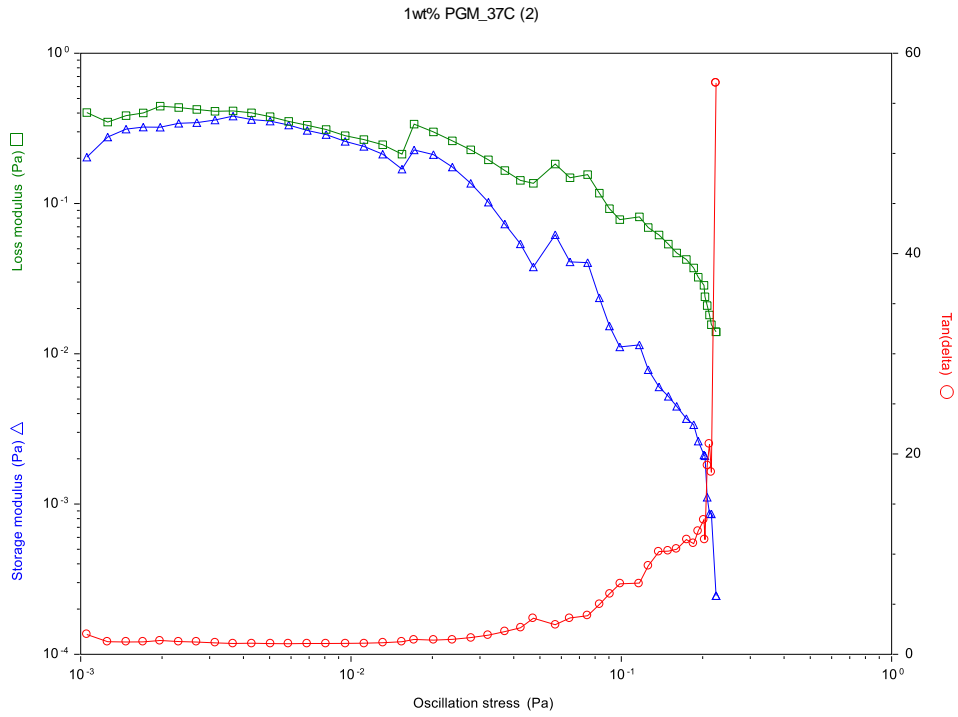


**Figure 38:** Dynamic stress sweep of 1 wt% PGM at 37 °C.

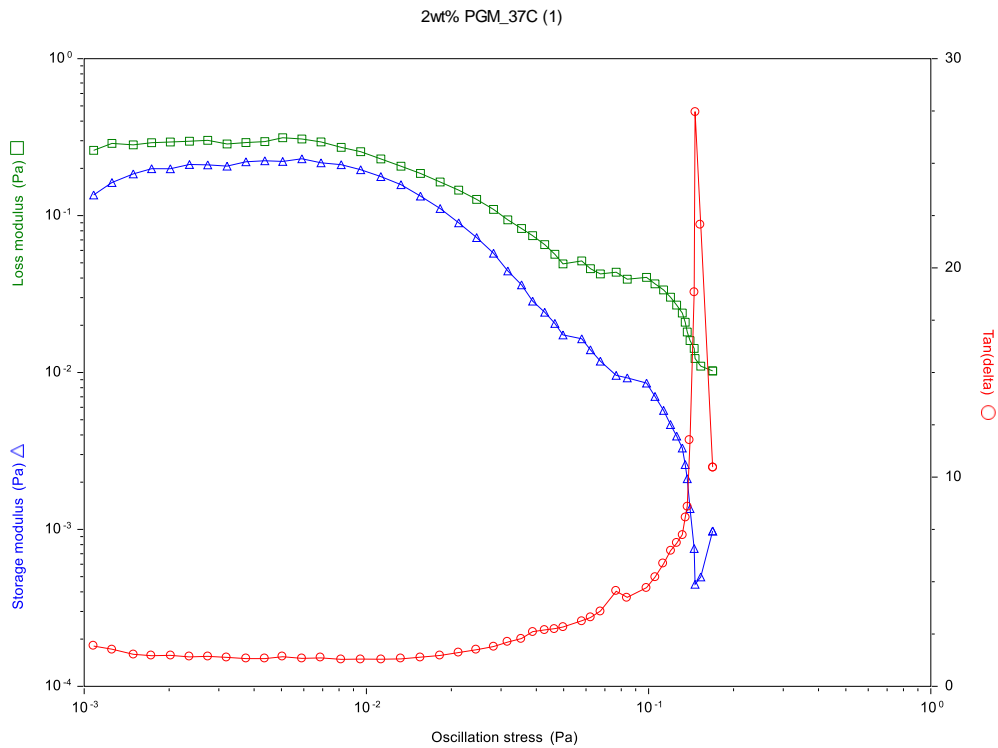


**Figure 39:** Dynamic stress sweep of 2 wt% PGM at 37 °C.

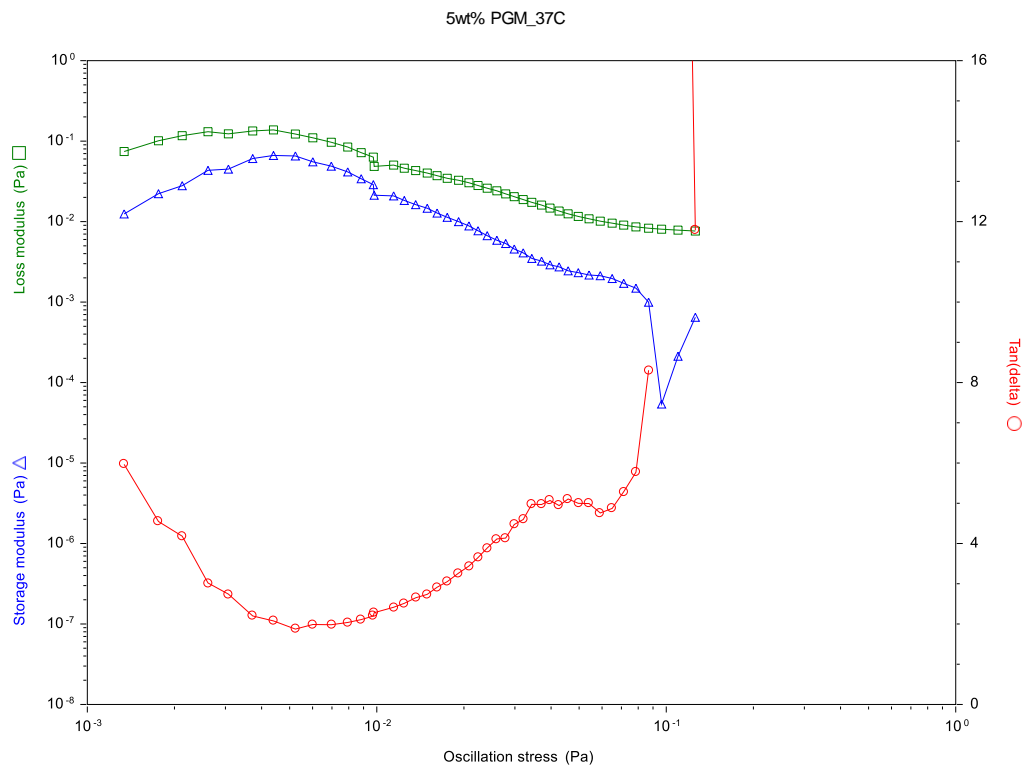


**Figure 401:** Dynamic stress sweep of 5 wt% PGM at 37 °C.

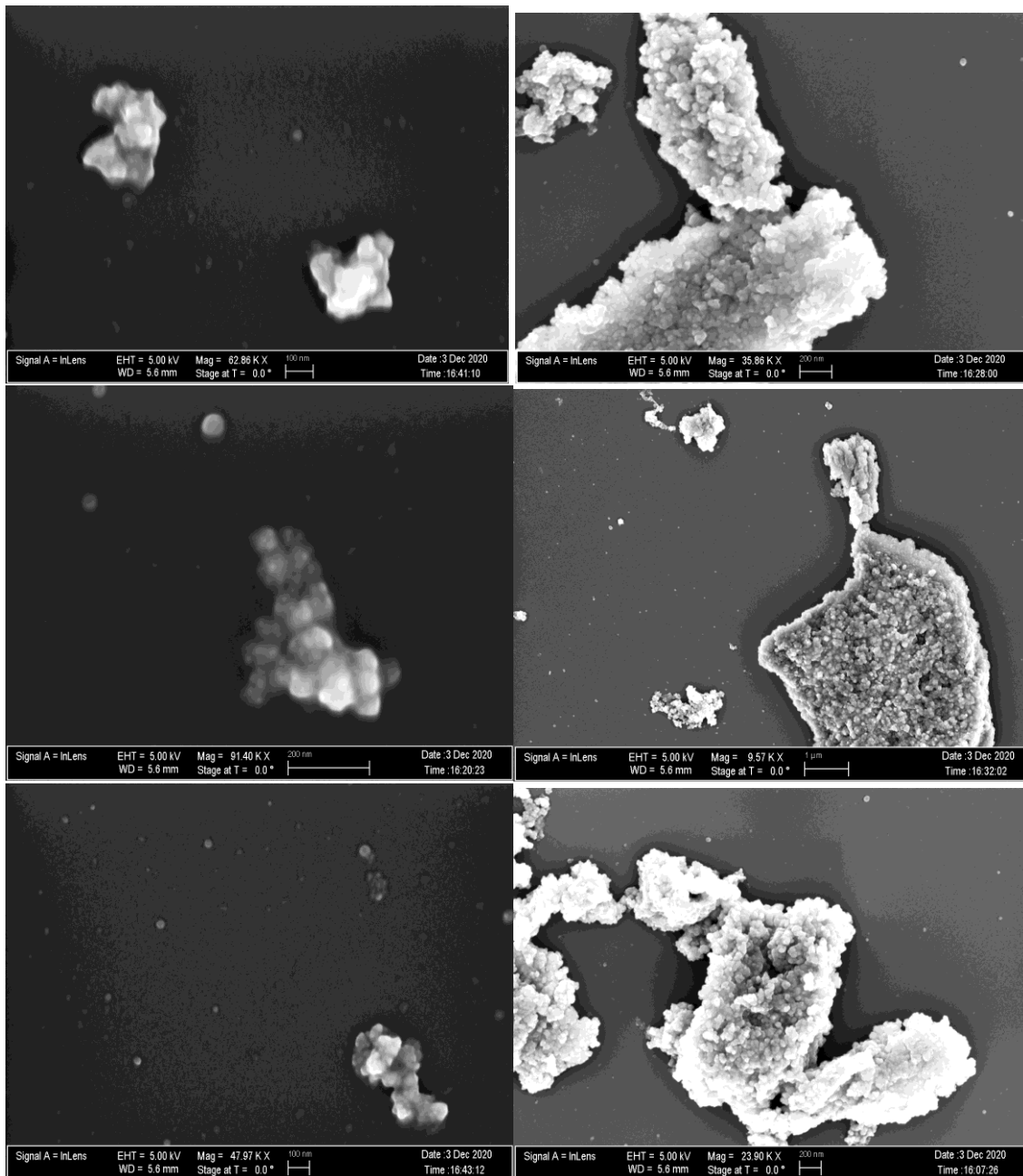


**Figure 41:** Magnetic nanoparticles imaged using SEM after filtering with 2 μm syringe filter.



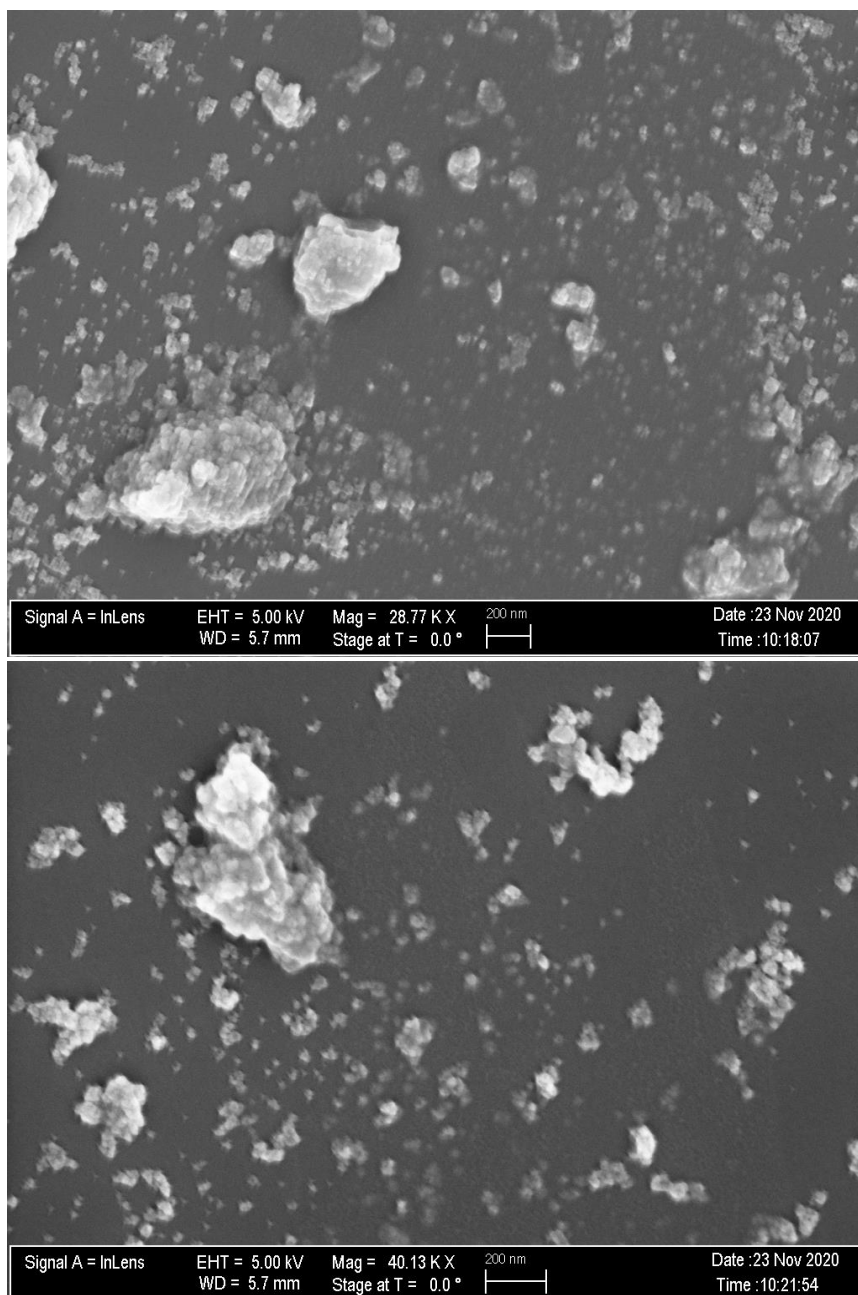


**Figure 42:** Unfiltered magnetic nanoparticles imaged using SEM before filtering with 2  $\mu\text{m}$  syringe filter.

		pH							
w t %	1	2	3	4	5	6	7	8	
5	SFT: --- ZP: (-0.9) mV D <sub>H</sub> : 255.61 nm	SFT: --- ZP: (-2.03) mV D <sub>H</sub> : 209.78 nm	SFT: 63.77 mN/m ZP: 0.39 mV D <sub>H</sub> : 729.90 nm	SFT: 62.62 mN/m ZP: (-7.9) mV D <sub>H</sub> : 408.74 nm	SFT: 61.73 mN/m ZP: (-13.4) mV D <sub>H</sub> : 195.94 nm	SFT: 56.71 mN/m ZP: (-14.23) mV D <sub>H</sub> : 181.37 nm	SFT: 54.30 mN/m ZP: --- D <sub>H</sub> : ---	SFT: 53.68 mN/m ZP: --- D <sub>H</sub> : ---	
2	SFT: --- ZP: (-0.79) mV D <sub>H</sub> : 202.27 nm	SFT: --- ZP: 0.16 mV D <sub>H</sub> : 325.31 nm	SFT: 66.82 mN/m ZP: (-1.76) mV D <sub>H</sub> : 933.93 nm	SFT: 66.26 mN/m ZP: (-6.67) mV D <sub>H</sub> : 235.55 nm	SFT: 65.20 mN/m ZP: (-18.9) mV D <sub>H</sub> : 171.34 nm	SFT: 60.14 mN/m ZP: (-22.15) mV D <sub>H</sub> : 209.171 nm	SFT: 56.34 mN/m ZP: --- D <sub>H</sub> : ---	SFT: 55.98 mN/m ZP: --- D <sub>H</sub> : ---	
1	SFT: --- ZP: (-1.24) mV D <sub>H</sub> : 238.93 nm	SFT: --- ZP: 1.46 mV DLS: 261.49 nm	SFT: 68.42 mN/m ZP: 0.01 mV D <sub>H</sub> : 766.61 nm	SFT: 67.42 mN/m ZP: (-7.12) mV D <sub>H</sub> : 612.27 nm	SFT: 67.26 mN/m ZP: (-12.19) mV D <sub>H</sub> : 138.05 nm	SFT: 61.80 mN/m ZP: (-17.12) mV D <sub>H</sub> : 218.75 nm	SFT: 59.39 mN/m ZP: --- D <sub>H</sub> : ---	SFT: 55.70 mN/m ZP: --- D <sub>H</sub> : ---	

**Figure 43:** PGM sol-gel transition ‘map’ showing the effect of pH and PGM concentration on PGM solution properties, including average SFT, ZP, and D<sub>H</sub> [■ = solution; ■ = gel; ■ = unknown].

## Works Cited

1. Samad, T.; Co, J. Y.; Witten, J.; Ribbeck, K., Mucus and Mucin Environments Reduce the Efficacy of Polymyxin and Fluoroquinolone Antibiotics against *Pseudomonas aeruginosa*. *ACS Biomaterials Science & Engineering* **2019**, *5* (3), 1189-1194.
2. Bansil, R.; Stanley, E.; Lamont, J. T., Mucin Biophysics. *Annual Review of Physiology* **1995**, *57* (1), 635-657.
3. Thornton, D. J.; Rousseau, K.; McGuckin, M. A., Structure and Function of the Polymeric Mucins in Airways Mucus. *Annual Review of Physiology* **2008**, *70* (1), 459-486.
4. Celli, J.; Gregor, B.; Turner, B.; Afdhal, N. H.; Bansil, R.; Erramilli, S., Viscoelastic Properties and Dynamics of Porcine Gastric Mucin. *Biomacromolecules* **2005**, *6* (3), 1329-1333.
5. Leon; Crouzier, T.; Sarkar, A.; Dunphy, L.; Han, J.; Ribbeck, K., Spatial Configuration and Composition of Charge Modulates Transport into a Mucin Hydrogel Barrier. *Biophysical Journal* **2013**, *105* (6), 1357-1365.
6. Caldara, M.; Friedlander, R. S.; Kavanaugh, N. L.; Aizenberg, J.; Foster, K. R.; Ribbeck, K., Mucin biopolymers prevent bacterial aggregation by retaining cells in the free-swimming state. *Curr Biol* **2012**, *22* (24), 2325-30.
7. Celli, J. P.; Turner, B. S.; Afdhal, N. H.; Keates, S.; Ghiran, I.; Kelly, C. P.; Ewoldt, R. H.; McKinley, G. H.; So, P.; Erramilli, S.; Bansil, R., *Helicobacter pylori* moves through mucus by reducing mucin viscoelasticity. *Proceedings of the National Academy of Sciences* **2009**, *106* (34), 14321-14326.
8. Curnutt, A.; Smith, K.; Darrow, E.; Vasquez, E. S.; Kundu, S.; Walters, K. B., Rheological Characterization of Mucus and Mucin Solutions in Response to pH and [Ca<sup>2+</sup>]. **2019**.
9. Vasquez, E. S.; Duggan, E. S.; Metcalf, J. P.; Kundu, S.; Walters, K. B. In *Examining Mucin Type and Morphology Effects on Mammalian Mucus Mechanical and Microstructural Properties*, Proceeding First Therm. Fluids Eng. Summer Conf.(Begellhouse, 2016).
10. Vasquez, E. S.; Walters, K. B.; Kundu, S., Nanoparticle-Biopolymer Effects on the Rheological Properties of Mucus, (in preparation), planned submission in *Biomacromolecules*.

11. O'Connell, A.; Smith, K.; Darrow, E.; Walters, K. B., Chemical and Microstructural Characterization of pH and [Ca<sup>2+</sup>] Dependent Sol-Gel Transitions in Mucin Biopolymer. *Scientific Reports* **2020**, *10* (1).
12. Zabet, M.; Mishra, S.; Boy, R.; Walters, K. B.; Naskar, A. K.; Kundu, S., Temperature-dependent self-assembly and rheological behavior of a thermoreversible pPAA–PnBA–PMMA triblock copolymer gel. *Journal of Polymer Science Part B: Polymer Physics* **2017**, *55* (11), 877-887.
13. Walters, K. B.; Kundu, S., "Examining Impacts of Nano- and Micro-Structures on Macro-Scale Fluid Rheology in Complex Fluids: A Mini-Review," (in preparation).
14. Vasquez, E. S.; Bowser, J.; Swiderski, C.; Walters, K. B.; Kundu, S., Rheological characterization of mammalian lung mucus. *RSC Adv.* **2014**, *4* (66), 34780-34783.
15. TA Instruments, Discovery Hybrid Rheometer – Quick Start e-Training Course. 2016.
16. Ramireddy, R. R.; Prasad, P.; Finne, A.; Thayumanavan, S., Zwitterionic amphiphilic homopolymer assemblies. *Polymer Chemistry* **2015**, *6* (33), 6083-6087.
17. Mystkowska, J.; Lysik, D.; Germaniuk, M.; Niemirowicz-Laskowska, K.; Bucki, R. In *The influence of pH and temperature on stability of artificial saliva based on porcine gastric mucin*, 2020; IEEE.
18. Hansen, C., "Solubility Parameters" in *Paint and Coating Testing Manual: 15th. ed of the Gardner-Sward Handbook*. *ASTM International* **2012**, 481-485.
19. Instruments, D., Surface tension values of some common test liquids for surface energy analysis.
20. LibreTexts, Map: A Molecular Approach (Tro). **2019**, *11*.
21. Porter, R. S.; Johnson, J. F., The Entanglement Concept in Polymer Systems. *Chemical Reviews* **1966**, *66* (1), 1-27.
22. Kočevár-Nared, J.; Kristl, J.; Šmid-Korbar, J., Comparative rheological investigation of crude gastric mucin and natural gastric mucus. *Biomaterials* **1997**, *18* (9), 677-681.
23. Hamed, R.; Fiegel, J., Synthetic tracheal mucus with native rheological and surface tension properties. *J Biomed Mater Res A* **2014**, *102* (6), 1788-98.
24. Celli, J. P.; Turner, B. S.; Afdhal, N. H.; Ewoldt, R. H.; McKinley, G. H.; Bansil, R.; Erramilli, S., Rheology of Gastric Mucin Exhibits a pH-Dependent Sol–Gel Transition. *Biomacromolecules* **2007**, *8* (5), 1580-1586.

25. Grillet, A. M.; Wyatt, N. B.; Gloe, L. M., Polymer gel rheology and adhesion. *Rheology* **2012**, *3*, 59-80.
26. Hasan, M. A., Rheological Behavior and Nano-Microstructure of Complex Fluids: Biomedical and Bitumen-Heavy Oil Applications **2010**.
27. Li, Q.; Zhou, J.; Zhang, L., Rheological behavior of cyanoethyl celluloses in aqueous solutions. **2012**, *19* (5), 1547-1555.
28. Cao, X.; Bansil, R.; Bhaskar, K. R.; Turner, B. S.; Lamont, J. T.; Niu, N.; Afdhal, N. H., pH-Dependent Conformational Change of Gastric Mucin Leads to Sol-Gel Transition. *Biophysical Journal* **1999**, *76* (3), 1250-1258.
29. Hong, Z.; Chasan, B.; Bansil, R.; Turner, B. S.; Bhaskar, K. R.; Afdhal, N. H., Atomic Force Microscopy Reveals Aggregation of Gastric Mucin at Low pH. *Biomacromolecules* **2005**, *6* (6), 3458-3466.
30. Lee, S.; Müller, M.; Rezwan, K.; Spencer, N. D., Porcine Gastric Mucin (PGM) at the Water/Poly(Dimethylsiloxane) (PDMS) Interface: Influence of pH and Ionic Strength on Its Conformation, Adsorption, and Aqueous Lubrication Properties. *Langmuir* **2005**, *21* (18), 8344-8353.
31. Maleki, A.; Lafitte, G.; Kjøniksen, A.-L.; Thuresson, K.; Nyström, B., Effect of pH on the association behavior in aqueous solutions of pig gastric mucin. *Carbohydrate Research* **2008**, *343* (2), 328-340.
32. Salgın, S.; Salgın, U.; Bahadır, S. In *Zeta Potentials and Isoelectric Points of Biomolecules: The Effects of Ion Types and Ionic Strengths*, 2012.
33. Patil, S.; Sandberg, A.; Heckert, E.; Self, W.; Seal, S., Protein adsorption and cellular uptake of cerium oxide nanoparticles as a function of zeta potential. *Biomaterials* **2007**, *28* (31), 4600-4607.
34. Salgın, S.; Takaç, S.; Özdamar, T. H., Adsorption of bovine serum albumin on polyether sulfone ultrafiltration membranes: Determination of interfacial interaction energy and effective diffusion coefficient. *Journal of Membrane Science* **2006**, *278* (1-2), 251-260.
35. Bansil, R.; Turner, B. S., The biology of mucus: Composition, synthesis and organization. *Advanced Drug Delivery Reviews* **2018**, *124*, 3-15.

36. Weigand, W. J.; Messmore, A.; Tu, J.; Morales-Sanz, A.; Blair, D. L.; Deheyn, D. D.; Urbach, J. S.; Robertson-Anderson, R. M., Active microrheology determines scale-dependent material properties of *Chaetopterus mucus*. *PLOS ONE* **2017**, *12* (5), e0176732.
37. M. Ways, T.; Lau, W.; Khutoryanskiy, V., Chitosan and Its Derivatives for Application in Mucoadhesive Drug Delivery Systems. *Polymers* **2018**, *10* (3), 267.
38. Li, C.; Liu, Z.; Yan, X.; Lu, W.; Liu, Y., Mucin-controlled drug release from mucoadhesive phenylboronic acid-rich nanoparticles. *International Journal of Pharmaceutics* **2015**, *479* (1), 261-264.
39. Chen, E. Y.; Daley, D.; Wang, Y.-C.; Garnica, M.; Chen, C.-S.; Chin, W.-C., Functionalized carboxyl nanoparticles enhance mucus dispersion and hydration. **2012**, *2*.
40. Lai, S. K.; O'Hanlon, D. E.; Harrold, S.; Man, S. T.; Wang, Y. Y.; Cone, R.; Hanes, J., Rapid transport of large polymeric nanoparticles in fresh undiluted human mucus. *Proceedings of the National Academy of Sciences* **2007**, *104* (5), 1482-1487.
41. Sun, D.; Kang, S.; Liu, C.; Lu, Q.; Cui, L.; Hu, B., Effect of zeta potential and particle size on the stability of SiO<sub>2</sub> nanospheres as carrier for ultrasound imaging contrast agents. *Int. J. Electrochem. Sci* **2016**, *11* (10), 8520-8529.
42. Wang, P.; Keller, A. A., Natural and Engineered Nano and Colloidal Transport: Role of Zeta Potential in Prediction of Particle Deposition. *Langmuir* **2009**, *25* (12), 6856-6862.
43. E.F. de la Cruz, Y. D. Z., E. Torres, W. Li, W.H. Song, K. Burugapalli, *Int J Electrochem* **(2012)** *7*,3577-3590.
44. Chen, E. Y. T.; Wang, Y.-C.; Chen, C.-S.; Chin, W.-C., Functionalized Positive Nanoparticles Reduce Mucin Swelling and Dispersion. *PLoS ONE* **2010**, *5* (11), e15434.
45. Dabbaghian, M. A.; Babalou, A. A.; Hadi, P.; Jannatdoust, E., A Parametric Study of the Synthesis of Silica Nanoparticles via Sol-Gel Precipitation Method. *International Journal of Nanoscience and Nanotechnology* **2010**, *6* (2), 104-113.
46. Gao, W.; Rigout, M.; Owens, H., Facile control of silica nanoparticles using a novel solvent varying method for the fabrication of artificial opal photonic crystals. *Journal of Nanoparticle Research* **2016**, *18* (12), 387.
47. Cristea, C.; Tertis, M.; Galatus, R., Magnetic Nanoparticles for Antibiotics Detection. *Nanomaterials* **2017**, *7* (6), 119.

48. Chem, Y. A. O. J., Magnetic Nanoparticles in Medicine: A Review of Synthesis Methods and Important Characteristics. **2015**, *31(Special Issue1)*.
49. Massart, R., Preparation of aqueous magnetic liquids in alkaline and acidic media. *IEEE Transactions on Magnetics* **1981**, *17* (2), 1247-1248.
50. Cheng, C.-L.; Chang, H.-H.; Chen, T.-H.; Tsai, P.-J.; Huang, Y.-T.; Huang, P.-J.; Lin, S.-Y., Spectral and morphological classification of different chronic and acute Taiwanese gallstones via FTIR, SEM and ESEM-EDX microanalyses. *Digestive and Liver Disease* **2016**, *48* (5), 519-527.
51. Pilling, M.; Gardner, P., Fundamental developments in infrared spectroscopic imaging for biomedical applications. *Chemical Society Reviews* **2016**, *45* (7), 1935-1957.
52. Biswas, N.; Waring, A. J.; Walther, F. J.; Dluhy, R. A., Structure and conformation of the disulfide bond in dimeric lung surfactant peptides SP-B1–25 and SP-B8–25. *Biochimica et Biophysica Acta (BBA)-Biomembranes* **2007**, *1768* (5), 1070-1082.
53. Ling, L.; Li, J.; Zhang, G.; Sun, R.; Wong, C.-P., Self-healing and shape memory linear polyurethane based on disulfide linkages with excellent mechanical property. *Macromolecular Research* **2018**, *26* (4), 365-373.
54. Sihota, P.; Yadav, R. N.; Dhiman, V.; Bhadada, S. K.; Mehandia, V.; Kumar, N., Investigation of diabetic patient's fingernail quality to monitor type 2 diabetes induced tissue damage. *Scientific reports* **2019**, *9* (1), 1-11.
55. Fathi Azarbayjani, A.; Jouyban, A., Surface tension in human pathophysiology and its application as a medical diagnostic tool. *BioImpacts* **2017**, *5* (1), 29-44.
56. Boya, V. N.; Lovett, R.; Setua, S.; Gandhi, V.; Nagesh, P. K. B.; Khan, S.; Jaggi, M.; Yallapu, M. M.; Chauhan, S. C., Probing mucin interaction behavior of magnetic nanoparticles. *Journal of Colloid and Interface Science* **2017**, *488*, 258-268.
57. Winkler, T., Determining the surface tension of liquids by measurements on pendant drops. *Tech. Note, KRÜSS* **2010**, 1-5.